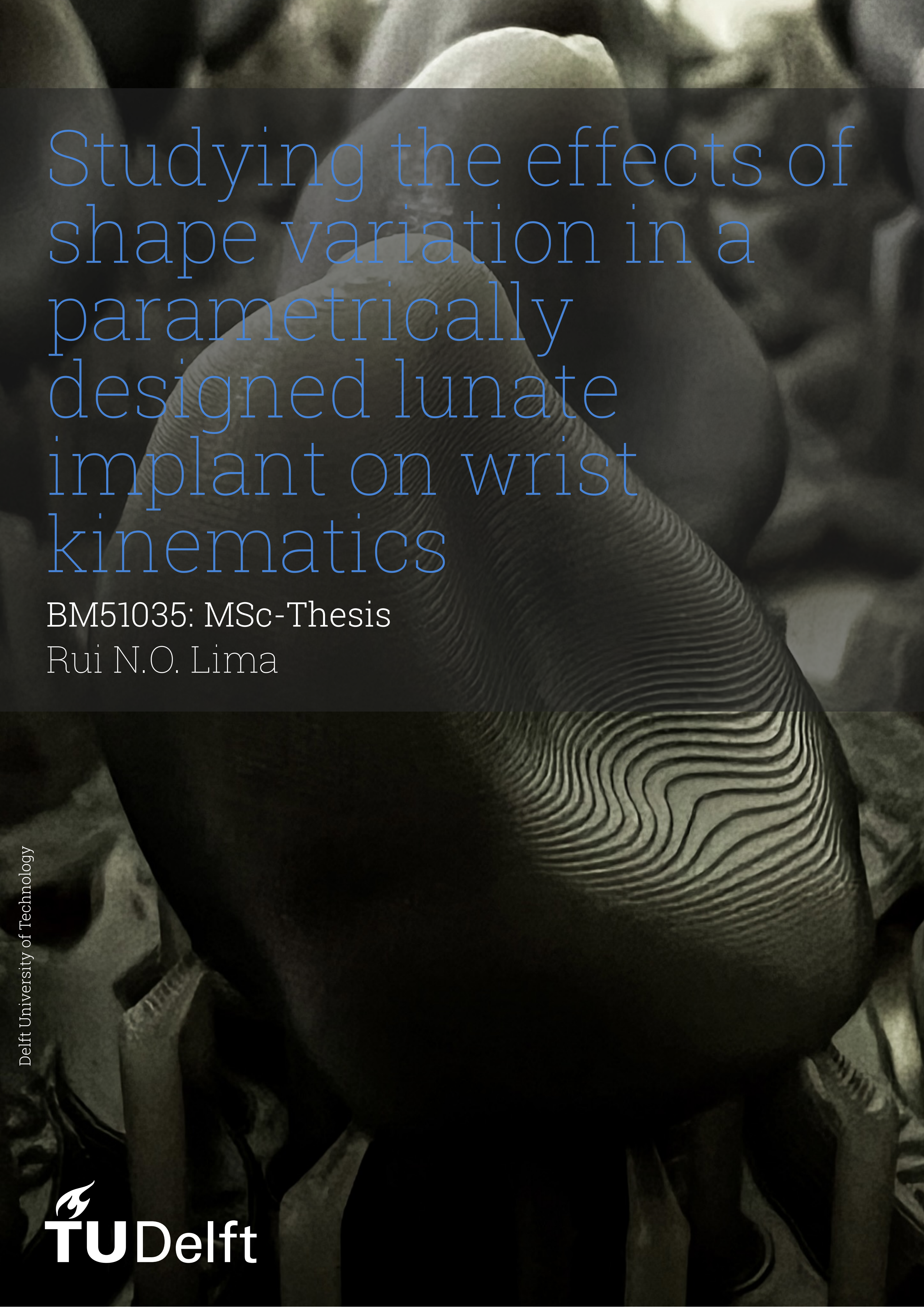

Studying the effects of shape variation in a parametrically designed lunate implant on wrist kinematics

BM51035: MSc-Thesis

Rui N.O. Lima

Delft University of Technology

Studying the effects of shape variation in a parametrically designed lunate implant on wrist kinematics

by

Rui N.O. Lima

Student Number:	5304083	
Faculty:	Faculty of Mechanical, Maritime and Materials Engineering	
Project Duration:	09/2022 - 05/2024	
Supervisors:	Dr. Ir. N. Tümer,	TU Delft
	Dr. G. A. Kraan,	Reinier Haga Orthopedisch Centrum
	Dr. J. van der Stok,	University Hospital Limerick

TU Delft

Preface

This thesis report is the culmination of my Master's degree in Biomedical Engineering at Delft University of Technology. This master's thesis explores the implementation of a statistical shape model approach in the development of a parametric lunate implant and the testing of lunate shape variations on wrist kinematics. I have been interested in the medical world since as long as I can remember, coming from a family of physicians. Seeing this world first-hand from a young age has inspired me to follow a career that not only is extremely interesting but is also rooted in a purpose to help people. When we add my passion for design to the mix, this project looked very appealing to me.

Before starting this project, I was unfamiliar with the complexity of the bones, ligaments, and tendons that make up the human wrist. When a carpal bone is compromised, due to trauma or a degenerative disease, an individual's hand function and overall quality of life can be severely affected. It is a challenging task to treat these problems, traditional treatment options often falling short in providing long-term relief. This is particularly true in the case of Kienböck disease, that affects the lunate bone. Motivated to understand the complexities of the wrist joint and discovering a treatment option that can improve the quality of life of those afflicted with injuries to the lunate bone, such as Kienböck disease, this project endeavors to conceptualize, design, and prototype a patient-specific lunate implant that not only replicates the kinematics of the natural lunate but also addresses how variations in lunate shape can influence the function of the wrist.

This has a been a challenging journey, involving countless hours of research, experimentation, and collaboration with other master students, researchers in the field, and clinical physicians. It gave me the opportunity to implement knowledge gathered from my academic education, but more so, the opportunity to learn multiple skills that better prepare me for my future endeavors. I deeply hope that the insights obtained from this project make a contribution to the advancement of medical device technology and improving the quality of life of those afflicted with lunate bone injuries.

I would like to thank my supervisor, Dr. Ir. Nazli Tümer for her invaluable support and guidance throughout my master's thesis. I would also like to thank Dr. Gerald Kraan and Dr. Johan van der Stok. Their expertise and guidance were instrumental in shaping my research. I would also like to thank Ian Bloom, the dedicated radiologic technologist at Reinier de Graff Hospital, for his crucial help during the experiments. Finally, I would like to extend my gratitude to my parents, family, and friends whose unwavering support and encouragement sustained me throughout this journey.

Rui N.O. Lima
Delft, May 2024

Summary

The wrist is one of the most complex joints in the human body, comprised of multiple bones and ligaments, and capable of performing a variety of movements. Proper wrist motion relies heavily on the interplay between the carpal bones of the hand and its ligamentous connections, and when that interplay is compromised hand function can be severely affected. Kienböck disease affects one of said carpal bones, causing the avascular necrosis of the lunate bone, located on the proximal carpal row (PCR). This disease ultimately leads to severe pain, carpal collapse of the lunate, and with it, loss of wrist function and quality of life. However, current treatment options do not meet the desired outcomes, lunate arthroplasty looking like a promising alternative.

This thesis presents the development of a 3D-printable parametric lunate implant and the study of the effects of shape variations on wrist kinematics, using a handheld motion guide device prototype and a CT Scanner. Kienböck disease is firstly introduced and the problems it causes to the lunate bone and surrounding bones are investigated, leading to the definition of the goals of this thesis. The development of a parametric lunate implant is then described, as well as the study of wrist kinematics, finishing with a discussion of the results. A statistical shape model (SSM) approach is used in the implant design, with a purpose to parameterize the design method and have the ability to apply it to various lunate shapes.

After an introduction, the implant requirements were firstly stated and the design approach was described. The parametrization of the implant design is then described, consisting of multiple Matlab codes and Solidworks macros to automatize the process. The resulting lunate implant design can be applied on any lunate implant shape variation described by the SSM. The necessary updates to the handheld motion guide device prototype are then specified, followed by a description of the experiment, looking into the embalmed human specimens used, the manufacturing of the lunate implants, and selection of shape variations to test. The experimental protocol was also clarified and the method used to post-process the experimental results. In the experiment, 3 modes of variation were tested and the effect of shape variations on wrist kinematics were assessed by measuring the scapholunate, radiolunate, and capitolunate angles.

The accuracy of the resulting lunate implant was tested on the SSM mean shape, deviations ranging between 0.00 and 0.13 millimeters. When it comes to the handheld motion guide device, the updates proved to improve the overall functioning of the device, albeit some issues were still encountered. The experiment showed one of the modes of lunate shape variation to have a significantly significant effect on wrist kinematics, t-tests for this mode showing p-values lower than 0.05. That could not be confirmed for the remaining modes tested.

To sum up, this thesis described the design of a lunate implant, showing that a statistical shape modeling approach is feasible in designing a parametric lunate implant. It also showed that one of the lunate shape variations have an effect on wrist kinematics. The implant design method shows promise for implementation in future designs and the knowledge gained from the experiment could be valuable to help us better understand the kinematics of the wrist.

Contents

Preface **i**

Summary **ii**

Nomenclature **iv**

1 Introduction **1**
1.1 Background 1
1.2 Research Objective 3

2 Methodology **4**
2.1 Design 4
2.1.1 Parametric Lunate Implant Design 4
2.1.2 Handheld Motion Guide Device Updates 7
2.2 Experiment 8
2.2.1 Specimens 8
2.2.2 Lunate Implants 9
2.2.3 Shape Mode Selection 9
2.2.4 Manufacturing of Lunate Implants for Experiment 10
2.2.5 Experimental Protocol 10
2.3 Post-Processing 11

3 Results **13**
3.1 Design 13
3.1.1 Parametric Lunate Implant Design 13
3.1.2 Handheld Motion Guide Device Updates 14
3.2 Experiment 15

4 Discussion **19**
4.1 Implant Design 19
4.2 Handheld device updates 20
4.3 Experiment and effects of lunate shape on wrist kinematics 21
4.4 Limitations 22
4.5 Conclusion 23

References **24**

A Experimental Protocol **27**

B Matlab Code **30**

C Solidworks Macros **31**
C.1 Spline Macro 31
C.2 Surface Macro 32

Nomenclature

Abbreviations

Abbreviation	Definition
CAD	Computer-Aided Design
CL	Capitolunate
DCR	Distal Carpal Row
FE	Flexion/Extension
LTIL	Lunotriquetral Interosseous Ligament
PCR	Proximal Carpal Row
PLA	Polylactic Acid
PMMA	Poly(methylmethacrylate)
RC	Radiocapitate
RL	Radiolunate
RUD	Radial/Ulnar Deviation
SD	Standard Deviation
SL	Scapholunate
SLIL	Scapholunate Interosseous Ligament
SSM	Statistical Shape Model

1
Introduction

1.1. Background

Kienböck disease, named after Austrian radiologist Dr. Robert Kienböck, also called avascular necrosis, osteomalacia of the lunate, or lunatomalacia, is a condition characterized by osteonecrosis of the lunate bone [1, 2]. The lunate bone is one of the eight carpal bones of the hand and located on the proximal carpal row (PCR), ulnar to the scaphoid bone, and radial to the triquetrum and pisiform bones. The carpal bones are shown in Figure 1.1. The carpal bones of the PCR are connected to the surrounding carpal bones through intrinsic ligaments and to the distal radius and ulna through extrinsic ligaments. There are no musculotendinous connections to the bones that comprise the PCR, all motion being caused by mechanical forces from the surrounding ligaments and articulations [3, 4]. Nevertheless, the PCR and its ligamentous connections, extrinsic and intrinsic, are of great importance for the kinematics of the wrist. Contrasting with the distal carpal row (DCR) bones, that are tightly bound to each other with limited movement between them, the PCR bones have significant movement between adjacent bones and act as an intercalated segment between the radius and the DCR, being responsible for wrist stability in any plane, including flexion and extension in the sagittal plane and radial and ulnar deviation in the coronal plane [3–5].

Multiple factors are considered to potentially cause Kienböck disease; however, the definite etiology of the disease is not yet fully understood. In the meantime, compartment syndrome of the lunate is thought to be the main cause of Kienböck disease, the resulting restricted blood supply leading to ischemia and consequent necrosis [6, 7]. Lunate hypertension is considered a risk factor for compartment syndrome of the lunate, caused by either venous obstruction or a lunate stress fracture. Moreover, Kienböck is mostly unilateral and 90% of patients are young male individuals with an active lifestyle, a probable factor being repetitive stress within this demographic [6].

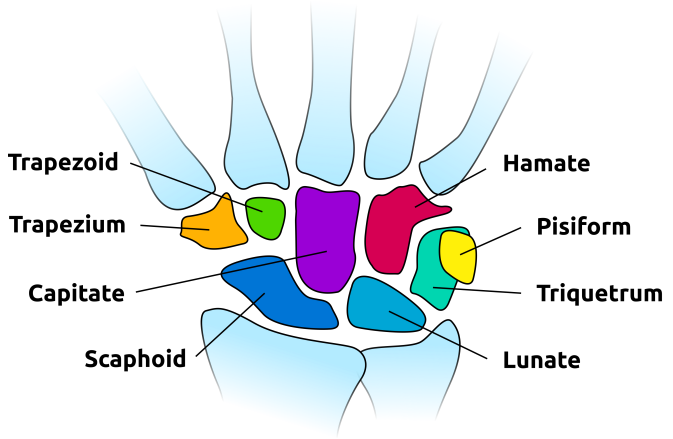

Figure 1.1: Carpal bones of the hand. Left hand anterior view.

Kienböck disease has been classified by Lichtmann into four stages, depending on changes on plain X-rays and MRI scans, stage I and stage IV being the least severe and most severe stages, respectively. Although the symptoms of wrist pain and the severity of this pain are not closely correlated with the Lichtmann stage, the Lichtmann stage is mainly important for direct treatment options. Stage I can be identified by uniformly decreasing signal uptake in MRI images, stage II by signs of sclerosis in X-ray images with changes in MRI, collapse of the lunate in stage III, and progressive carpal collapse in stage IV [2]. Stage III is also further divided into stage IIIA and stage IIIB, differentiated by a loss of carpal alignment and height, with capitate migration and scaphoid flexion being particularly noticeable. The stages of Kienböck disease are shown in Figure 1.2. Treatment of Kienböck disease is highly dependent on the stage of the disease, with multiple options available. Conservative non-surgical treatment is the go-to in stage I, consisting of 3 months of immobilization and anti-inflammatory medication [2, 7, 8]. The choice of treatment in stage II and stage IIIA, where the normal intercarpal relationship is maintained, depends on the variable anatomy of the patient's wrist, in particular the ulnar variance. The ulnar variance is described as the length of the ulna relative to the radius [9]. When there is a negative ulnar variance, treatment focuses on unloading procedures to reduce intracarpal stress and achieve revascularization, in which case surgeons prefer radial shortening and ulnar lengthening, where the radial and ulnar variances are leveled to modify the distribution of loads in the lunate [2, 8]. On the other hand, when there is a neutral or positive ulnar variance, there is no consensus regarding treatment, with core decompression, direct revascularization, and osteotomy procedures of the capitate amongst the options commonly described. Once the surrounding carpal bones are also affected, in stage IIIB and stage IV, the lunate can no longer be preserved and the treatment focuses mainly on restoring wrist function and minimizing pain. Surgery requires carpal bone removal, with proximal row carpectomy being a common procedure in which the entire proximal row is removed, or carpal bone fusion, with scapho-trapezio-trapezoid (STT) arthrodesis being a viable alternative, characterized by fusion of the scaphoid, trapezium, and trapezoid bones [2, 7, 8].

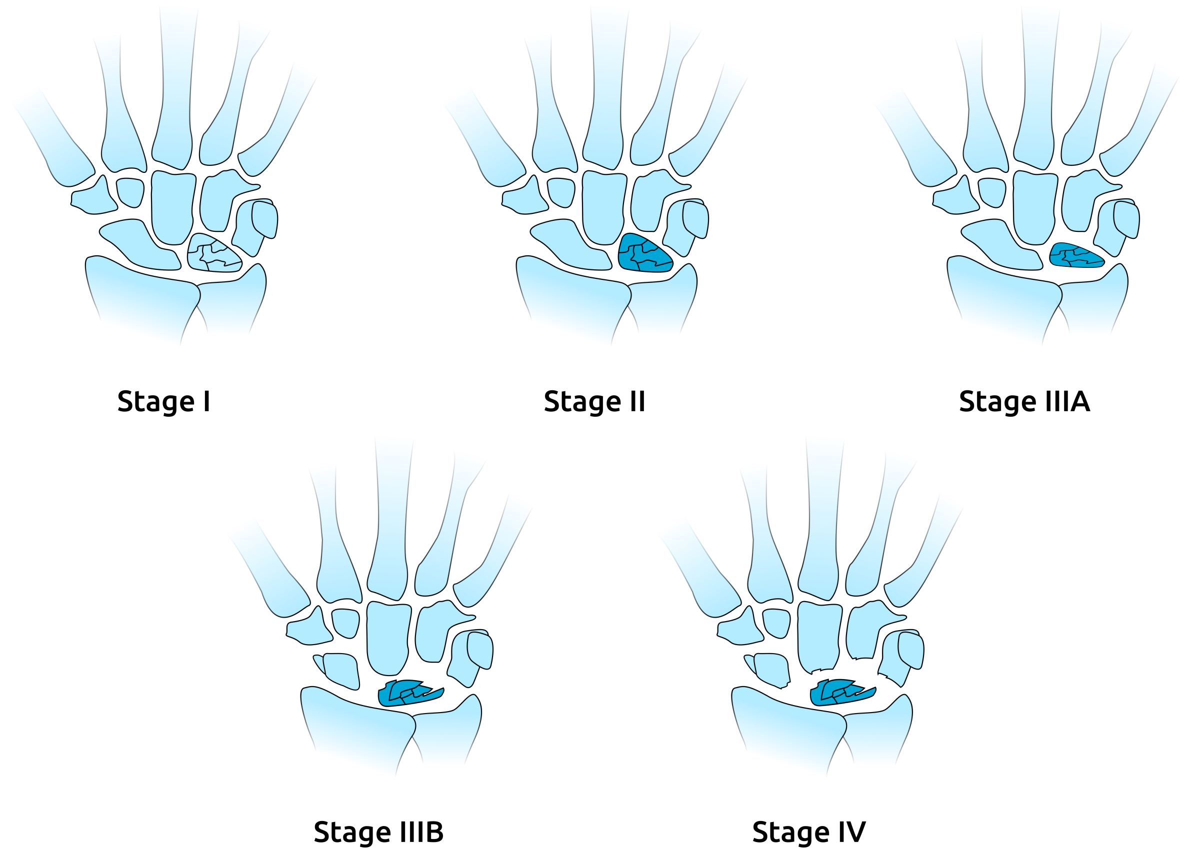

Figure 1.2: Stages of Kienböck disease. Left hand anterior view.

Meanwhile, the results obtained with current treatment options leave much to be desired, as they do not meet the desired functional requirements. For that reason, new approaches and methods are actively sought. A once-discarded method that shows promise due to recent technological advances is lunate arthroplasty. Lunate arthroplasty has been used to treat Kienböck disease since Swanson introduced the silicone implant in the 1970s, after attempts to use vitallium and acryl implants were unsuccessful [10]. Silicone lunate implants were soon abandoned, in the 1980s, due to cyst formation, implant dislocation, and development of synovitis caused by long-term release of silicone particles [10–13]. Then titanium and pyrocarbon implants were used, showing improved biocompatibility and mechanical properties; however, the generic shapes used today cannot fully restore wrist kinematics [10, 13–15]. Although this is the case, recent developments in 3D printing technologies and digital 3D software have made it possible to obtain patient-specific implants in a more affordable and timely manner, achieving a shape that more accurately resembles the lunate of the patient, and arguably matching the mechanical properties of the implant with the mechanical properties of the lunate bone of the patient [16]. This process requires scanning the patient's lunate bone, but given that the affected lunate loses its original shape, the unaffected contralateral lunate must be used as it is generally assumed to be the best fit. Yet, as identified by Tümer using a three-dimensional (3D) statistical shape modeling (SSM) approach, lunates are not bilaterally symmetrical in certain shape variations, demonstrating that intra-subject shape variations in the lunate can be comparable to those of inter-subject [14]. However, it is still uncertain whether and how the shape of the contralateral lunate and associated shape deviations affect the kinematics of the wrist.

1.2. Research Objective

The goal of this thesis is to design a 3D-printable parametric lunate implant based on the 3D SSM of the lunate developed by N.Tümer [14], vary its shape and experimentally study the effects of shape on wrist kinematics. The thesis goals can be translated into the following research questions:

1. **What is the feasibility of using a statistical shape modeling approach in designing a parametric lunate implant?**
2. **How do shape variations in the lunate implant affect the wrist kinematics?**

This thesis will contribute to further development of 3D printed patient-specific carpal bone implants, lunate implants in particular, by studying these questions.

The methods used to design and manufacture a parametric lunate implant, to perform an experiment, and to post-process experimental data will be detailed in Chapter 2, and the study outcomes will be shared in Chapter 3. The thesis report will end with discussion and conclusion in Chapter 4.

2
Methodology

This chapter describes the approach towards the design of a parametric lunate implant and the updates to the motion guide device, as well as the methods to both retrieve wrist kinematics data and post-process it. The design process is first described in Section 2.1. The experimental protocol and setup are explained in Section 2.2. Lastly, the post-processing methods are described in Section 2.3.

2.1. Design

2.1.1. Parametric Lunate Implant Design

The 3D SSM was developed by N.Tümer [14] using a point-cloud based approach. Using such a point-cloud based model, it is possible to generate a geometrically accurate tessellated model of the lunate with 3D triangle meshes. Meanwhile, this type of surface, although geometrically accurate, poses challenges to implant design, as it is not suitable for further geometric manipulation and is not well supported by popular computer-aided design (CAD) software packages [16, 17]. Most of the available CAD operations are spline-based, allowing a consistent surface patch layout [17]. Therefore, a spline-based approach was favored for the parametric implant design.

Furthermore, the point cloud obtained with the SSM has a total of 20,446 corresponding points. An image of the mean lunate shape with the 20,446-point corresponding points is shown in Figure 2.1. This is a high number of points, which even though able to present the most accurate representation of the lunate shape, it also makes it cumbersome to use in the design process. Consequently, a reduction of the number of points in the point-cloud into a more manageable size but still able to effectively represent the lunate shape was necessary. Moreover, once the attainment of the simplified point cloud was parameterized, the spline and surface creation was also to be automatized in order to easily obtain not only the point cloud but also a fully designed implant. Thus, the requirements for the implant design were as follows:

- Use a spline-based design approach
- Significantly reduce the number of points used
- Automatize the implant construction from the point cloud

Taking into consideration the aforementioned requirements for the implant design, a spline-based approach was used on the design process, using the mean shape of the lunate SSM as a template. Due to the fact that the mean shape has a relatively smoother surface, but still contains the characteristic features of the lunate shape, the mean shape was considered a good starting point for the spline-based design approach [17]. The approach consisted of designing a series of splines that follow the contours of the mean lunate mesh shape, generated as a tessellated model from a 20,446 point cloud. These splines were then used to create surfaces that can be patched into a solid body, representing the full shape of the lunate as closely as possible. All required implant modeling was performed using SOLIDWORKS® CAD software (version 2021 SP5.0, Education Edition, Dassault Systèmes SolidWorks Corp, Waltham, Massachusetts, USA) set to default settings. All splines were created using the spline command, and all surfaces were created using the Boundary Surface and Filled Surface commands in Solidworks. The boundary surface command was preferred as it offers more control, creating a surface from a selection of profiles in one or two directions [18]. However, it is not suitable for surfaces with 2, 3 or 5 + sides, as it leads to a problem called 'degenerate point', where the two edges of the surface converge in a single vertex. The surface fill command is more suitable for this type of surface since it generates a 4-sided surface and trims it to fit within the patch boundary, solving the "degenerate point" problem but offering less surface control [18]. Both surface commands in Solidworks use approximating lofting techniques, which create the surface on an approximated set of points based on the spline points and curves with a certain accuracy [19].

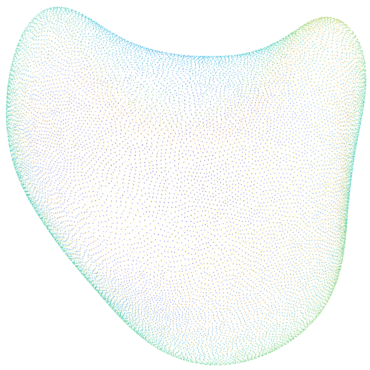

Figure 2.1: Point cloud of mean lunate with 20,446 total points obtained from the SSM.

The design process started by generating a tessellated model of the mean lunate with 3D triangle meshes. This was achieved by opening the SSM-derived mean point-cloud in Solidworks as a point-cloud and automatically generating a tessellated model using Mesh Prep Wizard, keeping the original orientation and point-cloud size. The tessellated model of the mean lunate with 3D triangle meshes is shown in Figure 2.3. Once the mean shape was obtained, it was important to decide how the shape should be segmented to facilitate surface generation using the CAD software (Solidworks). Particular attention was paid to avoiding surfaces with 2 and 3 sides as much as possible, since as previously stated, these can cause problems when using the Boundary Surface command and decreased surface control when using the Filled Surface command [18]. On that account, the implant was segmented into a total of six surfaces, with the boundary splines of these surfaces placed in selected areas of interest or anatomical landmarks. The placement of the boundary splines was defined with three sagittal planes (one through the center of the lunate and two through the distal poles of the lunate) and two axial planes (both below the curvature of the distal side of the lunate). The boundary splines were created on the five described planes, delineating the six surfaces. The way the surfaces were segmented is shown in Figure 2.2 and the boundary splines on Figure 2.3. It was not possible to avoid having two two-sided surfaces (red and blue zones in Figure 2.2).

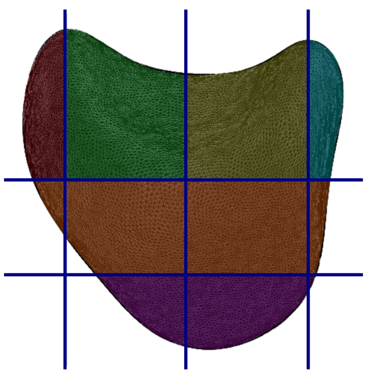

Figure 2.2: Method to segment the implant design into 6 surfaces. Each colored section represents one surface.

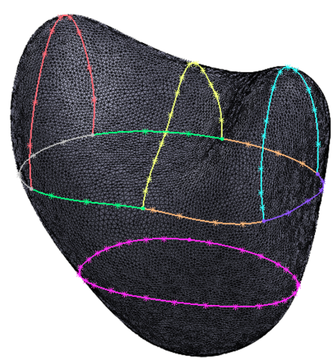

Figure 2.3: Surface boundary splines on tessellated model of the mean lunate. Each color represents one spline/sketch.

The boundary splines alone are not enough to recreate the shape of the lunate, so more splines were necessary. Therefore, multiple planes were added to the design to create the splines. All splines were created out of planes parallel to either the sagittal, coronal, or axial planes, using the same method as the previous splines. All connecting splines were made tangent to each other to ensure continuous surface connections. A total of 81 splines were used in the final design. The entire spline network is shown in Figure 2.4. Once the splines were set, these were used to create the surfaces. Different surface commands were used depending on the shape and number of sides of the surface, boundary surface being used for 4-sided surfaces and surface fill for the rest [18]. Contact edge settings were used in all surfaces, as well as surface optimization within Solidworks. The surfaces were knitted using the Knit Surface command, selecting the merge entities and create solid settings. The final design had a total of 719 points, meaning a resulting 97% point cloud size reduction. The design is shown in Figure 2.5.

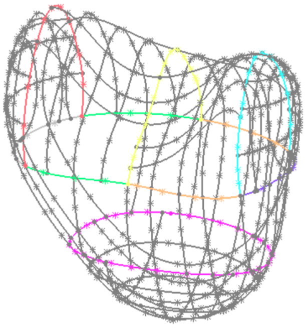

Figure 2.4: Entire spline network used on the implant design.

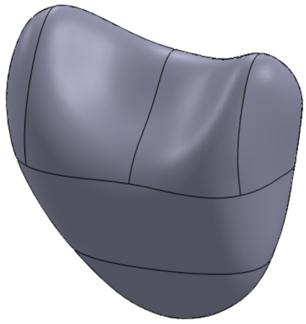

Figure 2.5: Implant design composed of 6 patched surfaces.

Although the number of points used was significantly reduced, the design still required a large number of splines and commands, making the design process cumbersome and ineffective to perform manually for multiple shapes. Therefore, it was necessary to automatize this process so that it could be easily applied to the remaining lunate shapes described by the SSM. Moreover, the coordinates of the points used should be replaced by the coordinates of points from the SSM to increase accuracy and facilitate changing of lunate shape. Automatization of the described design process was achieved using Macros in Solidworks, and any SSM related coding was done using MATLAB® ((R2020b), The MathWorks Inc., Natick, Massachusetts, USA).

The first step of the parametrization process required matching the points used in the design with points from the 3D SSM of the lunate. To do this, all points used in the design were selected, copied into a new Solidworks document, and saved as an IGS file. This allowed one to collect the 3D coordinates of the points and import them into MATLAB. The coordinates were saved as a 719x3 matrix, while the SSM coordinates are presented as a 20,446x3 matrix. Once imported into MATLAB, the closest points on the SSM were obtained using a simple dsearchn command. It finds within the coordinates of the SSM mean shape the IDs of the nearest points to the points used in the implant design in Euclidean distance, which in mathematics is the length of the line segment between them [20].

Once the IDs of the needed SSM points were retrieved, these could be used to obtain the necessary coordinates of the 719 points for every lunate shape described by the SSM, including the mean, since the IDs of the points do not change regardless of the SSM shape used. The 3D coordinates of a particular lunate in the SSM population can be described as follows:

$$x = \bar{x} + \sum_{s=1}^{c} b_s \phi_s \tag{2.1}$$

where x describes the 3D coordinates of the new bone, $\bar{x}$ describes the coordinates of the mean shape of the bone, the values of b_s describe the contributions of the first c modes of shape variation, and ϕ_s describes the first c modes of shape variation [21]. Therefore, the coordinates of the points with the retrieved IDs could be altered by changing the b values for the corresponding modes of shape variation. A MATLAB code was written for this and can be found in Appendix B.

After being able to obtain the 3D coordinates of the 719 points for any chosen lunate shape, the implant design process was repeated, this time automating it using Solidworks macros. The coordinates of the mean shape (719x3) were exported from MATLAB as a .txt file and imported into Solidworks as a sketch, to allow the selection of each point separately. Simply opening the file, as done before, would lead the software to read the .txt file as a point cloud, making it impossible to use each point separately, which is necessary for spline creation. To import it as a sketch, a first macro was written. This macro opens the point cloud as a sketch, one point at a time, from an already opened part in Solidworks, and fixes all points so that they are not accidentally moved. Each point has an ID in the software from 1 to 719.

Once the points were imported, the splines could be recreated, with one macro being written for the generation of each spline, using the IDs of the points to define how the spline is designed. Given that there were 81 splines in the preliminary implant design, 81 macros were created to rebuild the spline network, followed by another macro to run them all in succession. Once all the splines are created, the surfaces were also created using one macro for each surface, six in total. The last surface macro also patches the surfaces using the Knit Surface command. A macro was also created to perform the six surface macros in succession, finishing the automatization of the implant design process. A total of 90 macros were used in this process; however, only three macros must be manually selected to obtain a lunate implant: one to import points, one to create all the splines, and one to create the surfaces. Examples of each macro used are shown in Appendix C. The lunate implant designs are shown in Figure 2.6.

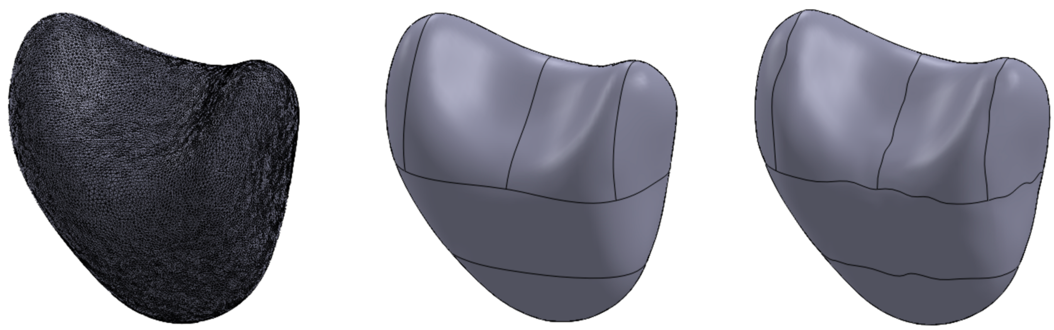

Figure 2.6: Mean lunate from SSM: initial mesh lunate with 24,446 points (left), preliminary implant design obtained with points close to the mean lunate shape (center), and automatized implant design obtained with SSM coordinate points (right).

2.1.2. Handheld Motion Guide Device Updates

The assessment of the kinematics of the wrists was to be done with a previously developed handheld motion guide device. This device was developed by a TU Delft master student and further tested by a student from The Hague University of Applied Sciences, and relies on two stepper motors that drive two timing belts, which are responsible for moving the handheld part of the device [22, 23]. It performs two types of motion, flexion / extension (FE), more specifically neutral position to flexion, and ulnar/radial deviation (RUD). However, certain issues were encountered during tests performed by previous master students that prevented consistent use of the device for wrist kinematics testing. The device is shown in Figure 2.7, which highlights some of its features.

During previous tests performed with the device, it was observed that the side timing belts (Fig. 2.7.E) were too loose, resulting in insufficient force to perform the required motions. Another issue, was that the pulleys of the timing belts (Fig. 2.7.D) were not aligned, causing the belt to not work efficiently. Furthermore, the force applied to the belts caused the nylon screws (2.7.f) that connected the pulleys to bend, preventing the device from performing the movements correctly and damaging the device. Therefore, some updates on the device were required before testing.

The technical drawings of the previous hand-held device were made available by the former TU Delft master student. Most of the parts in the device had been designed using SOLIDWORKS® CAD software (version 2021 SP5.0, Education Edition, Dassault Systèmes SolidWorks Corp, Waltham, Massachusetts, USA) and laser cut from transparent PMMA in the student workshop of the Faculty of Mechanical,

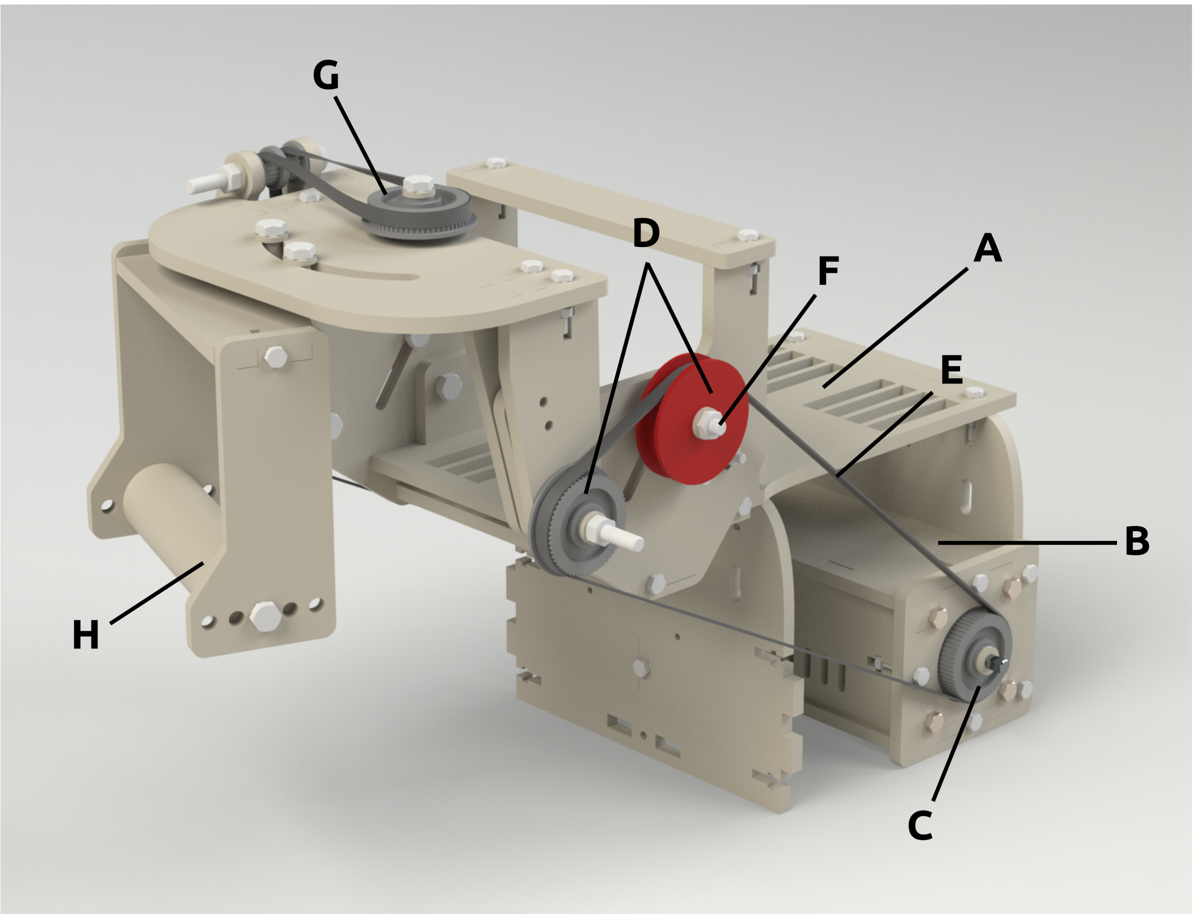

Figure 2.7: Handheld Motion Guide Device. A) Plateau where the arm rests. B) Housing for the stepper motors. C) Gear from stepper motor. D) Timing Belt Pulleys for FE. E) Timing Belt. F) Nylon screw that fixes the pulley to the device. G) Timing Belt Pulley for RUD. Edited from [22].

Maritime and Materials Engineering (ME) of TU Delft [22]. 3D printing with a FDM modified Creality Ender 3 printer (Creality, Shenzhen, China) and eSun PLA+ filament (Shenzhen Esun Industrial Co., Ltd., Shenzhen, China) was also used for some parts. To manufacture the updated parts, the same software and manufacturing techniques were used, with the exception that a FDM Prusa i3 MK3S (Prusa Research, Prague, Czech Republic) with recycled PLA was used for 3D printed parts.

2.2. Experiment

An experiment was set up with two embalmed human specimens in order to evaluate the effects of lunate shape variation on wrist kinematics. For each specimen, multiple lunate implants modified by different shape modes and standard deviations, , *i.e.*, b values in Eq.2.1, were tested by performing two types of wrist motion, flexion / extension (FE) and radial / ulnar deviation (RUD), with the handheld motion guide device. The samples were scanned with a 4D CT machine during each test.

2.2.1. Specimens

Two embalmed human forearm specimens (including the elbow) were used in the experiment. The specimens were made available to the study by the Erasmus University Medical Center, with the approval of the medical ethics committee of the Reinier Haga Orthopedic Center (RHOC). Two samples were tested given the limited time frame for the experiment and the relatively high amount of tests performed per sample. The specimens were inspected for wrist injuries or pathologies.

2.2.2. Lunate Implants

The 3D SSM allows one to tailor the design of the implant to the lunate of a particular individual. Given that one of the objectives of this study is to test the effect of lunate shape variations on the kinematics of the wrist, creating patient-specific implants for each available embalmed specimen in the experiment permits a more accurate comparison with the original lunate, also permitting testing of one shape variation at a time by modifying its particular b value. Consequently, using the SSM and the parametric design pipeline for each specimen, patient specific implants were designed for the two specimens.

Static CT scans of the available embalmed specimens with intact lunate bones were acquired in a previous experiment performed by a student from The Hague University of Applied Sciences [23] and were made available for this study. The scans were imported into 3D Slicer (Version 5.6.0), where the lunate bones of each sample were segmented. The thresholding technique was used in the bone segmentation process, using the 3D Slicer Segment Editor module, which semi-automatically creates a segmented volume. This method was applied to the area of the scan where the lunate bone is. Bone boundary inaccuracies were manually corrected, followed by surface optimization using the Smoothing command. The segmented volume was then saved for each sample and exported as standard tessellated (STL) files.

Finally, the STL files were opened on MeshLab (version 2016.12, CNR, Rome, Italy), where a point cloud was generated for each sample. A code provided with the SSM, was used to generate the fitting parameters (b-values) for each sample. The code uses the mean shape and modes of variation of the SSM to fit it to a point cloud. The fitting parameters allowed us to generate patient-specific implants for the two embalmed human specimens that could be modified with any mode of shape variation in the SSM. It was, however, necessary to decide which shape modes were to be tested.

2.2.3. Shape Mode Selection

Referring to the study by Tümer [14], 13 shape modes described by the SSM were viewed. Of the 13 shape modes, three were selected for testing. The first selected shape mode was shape mode 1, which describes a shape variation on the volar or dorsal side of the lunate and the curvature of the proximal side, which articulates with the radius. Moreover, the volar shape variation in this shape mode is directly related to Watson's classification of D-, V-, and N-type lunates, D-lunates featuring a thinner dorsal segment, V-lunates a thinner volar segment, and N-lunates equal dorsal and volar segments [14, 24]. This mode was selected due to its contribution to total shape variation, as it has the highest contribution among all the shape modes at 11%.

The second selected shape mode was shape mode 3, which describes a shape variation on the angle between the radial side, which articulates with the scaphoid, and the proximal side, that articulates with the radius on the volar side. The described angle is the main distinguishing factor in Antua Zapico's classification of lunates A-Z types I, II, and III, type I having an angle greater than 130°, type II having an angle of approximately 100 °, and type III having two distinct facets on its proximal surface [14, 25, 26]. Mode 2 was selected because even though its effects on the biomechanics of Kienböck disease have been previously described in various studies [27, 28], no reports were found on its effects on wrist kinematics.

The third and final shape mode selected was shape mode 13, which describes a shape variation on the curvature of the bone surface articulating with the capitate. The shape mode 13 was selected due to the absence/presence of a distal articular ulnar facet that aligns with Viegas's classification of V-Type I or II lunates [14, 29]. These two types of lunates were shown to affect wrist kinematics during the flexion/extension motion, which makes shape mode 13 relevant for testing [30, 31]. The three selected shape modes and the shape variations described by them are represented on the mean lunate shape in Figure 2.8.

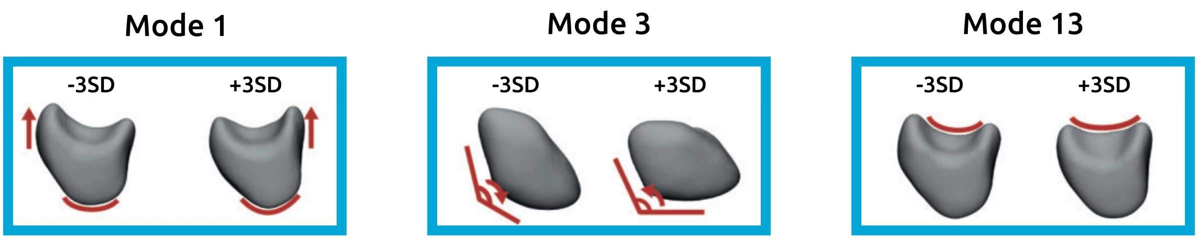

Figure 2.8: Shapes modes selected for testing. The shape variations are shown on the mean lunate shape. Edited from [14].

Referring to the study by Tümer [14], the values of the modes of shape variation, eigenvalues in the SSM, were shown to have a distribution varying between -3 and +3 standard deviations. Therefore, 3 standard deviations (SD) were added and subtracted from the shape parameters representing the selected shape modes, resulting in two implants for each shape mode, one with +3SD and one with -3SD.

2.2.4. Manufacturing of Lunate Implants for Experiment

The lunate shapes to be tested were printed using an SLA Formlabs Form3 3D printer (Formlabs, Somerville, MA, USA) at the Employee Walk-In Workshop of the Faculty of Mechanical, Maritime, and Materials Engineering (ME) of the TU Delft. It was printed using Form Tough 1500 Engineering Resin (Formlabs, Somerville, MA, USA), which is CT compatible. The implants were manufactured using a plastic material because given that the experiment was set up with embalmed human specimens, there were no biocompatibility requirements, so there was no need to use a biocompatible material such as titanium. SLA was selected over FDM (fused deposition modeling) due to its high precision in small parts and smoother surface finish due to lower forces applied during the printing process [32]. Moreover, this 3D printing method results in isotropic parts, meaning that the strength of the parts does not change with orientation [32]. The parts where therefore oriented in the way that allowed to print them all simultaneously to reduce printing time.

2.2.5. Experimental Protocol

The experiment was setup with a Toshiba Aquilion One CT scanner (Canon Medical Systems Corporation, Otawara, Tochigi, Japan) at Reinier de Graaf Hospital in Delft. The CT scanner was operated by a radiotechnician from the same hospital. The handheld motion guide device was attached to a wooden board using holes and zip ties and was properly padded with absorbent pads to prevent leaks or damage to the electronic components of the device. This is shown in Figure 2.9.

The two embalmed human specimens were collected by the hand surgeon, Dr. G.A. Kraan, who also performed the surgeries to excise the original lunates and insert the implants to be tested. Briefly, a dorsal wrist approach was used, opening the 4th extensor compartment and subsequently opening the dorsal wrist capsule via a Berger flap. The scapholunate and lunotriquetral ligament were incised to allow for explantation of the native lunate. After implantation, the dorsal wrist capsule was closed with interrupted nylon sutures. The specimens were secured to the device using elastic straps. An image of an embalmed human specimen with a lunate implant inserted is shown in Figure 2.10.

The specimens and the corresponding implants were tested in two types of motion, flexion / extension (FE) and radial / ulnar deviation (RUD), using the handheld motion guide device. The device was set to perform FE motion from neutral position to 80º of flexion and RUD motion from 34º to -34º [22]. When it comes to CT scanning parameters, the settings were constant throughout the experiment. Radiation dose was set to a tube current of 80 mA, as this is a commonly used value for this type of scan and the value used in previous experiments [22, 33]. The scan duration was set to 12.75 s with a reconstruction time of 0.25s, to once again match previous experiments. A radiotechnician from Reinier de Graaf Hospital in Delft was also consulted for the selection of these settings. The experimental protocol used during the experiments is included in Appendix A.

Each test was repeated 3 times, each implant being therefore scanned 6 times, 3 on the FE motion and 3 on the RUD motion. A total of 7 implants were tested per specimen, comprising of the mean shape and the specimen's lunate shape with +/- 3SD in the three selected shape modes, resulting in a total of 42 scans per specimen. When all tests with an implant were complete, the specimen was removed and the implant replaced. The surgeon applied a suture on site each time the implant was inserted to prevent the implant from moving. Since the original lunates had been excised at the Erasmus Medical Center Wet lab, scans from a previous experiment on the healthy lunates of the specimens were used to compare the kinematics of the wrist with and without the implants. The scans taken of the healthy lunates were taken only once.

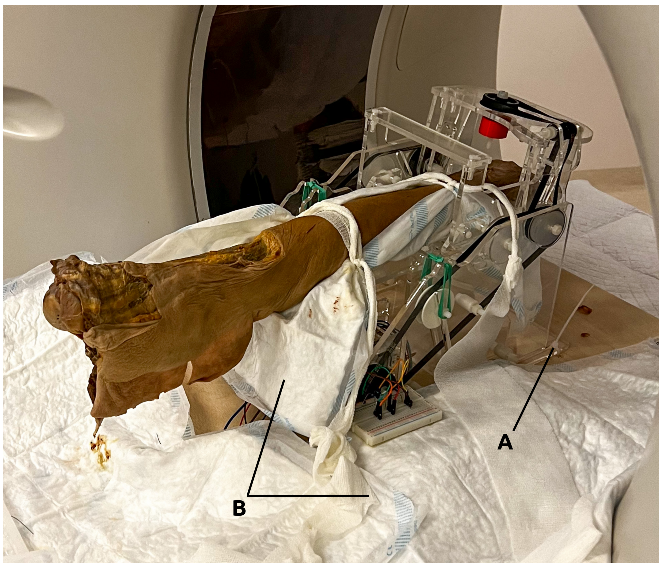

Figure 2.9: Embalmed human specimen strapped to the handheld device. A) Zip ties used to attach the device to the wooden board. B) Absorbent pads.

Figure 2.10: Embalmed human specimen with a lunate shape implanted. (A) Lunate implant.

2.3. Post-Processing

During the experiment, the 4D CT scans were named and saved for easier identification and exported as DICOM images, each 4D CT scan representing one test and consisting of a series of frames. To visualize the images, these were imported into 3DSlicer (Version 5.6.0). For each FE test, the frames in which the wrist is on maximum flexion were selected in order to assess intercarpal kinematics but also the overall flexion of the wrist. For each RUD test the frames where the wrist is on maximum ulnar and radial deviation had to be selected.

Various metrics were selected for evaluation. For future comparison with data obtained from a previous TU Deft master student project concerning carpal instability, the capitolunate (CL) and scapholunate (SL) angles were to be obtained. Moreover, to evaluate FE, the radiolunate (RL) angle was to be obtained, and for RUD, the radiocapitate (RC) angle. The CL, SL, and RL are clinically evaluated using a lateral view, while the RC angle is evaluated using a postero-anterior view [34]. Consequently, three slices were saved for each FE test where the lunate, capitate, and scaphoid are most visible, all of these on a lateral view where the wrist is at its maximum flexion. For the RUD tests, two slices were taken in positions where the capitate and radius are most visible, both on a postero-anterior view where the wrist is at its maximum ulnar deviation and maximum radial deviation. The selected slices were then opened and the needed angles were measured on ImageJ (version 1.53, Wayne Rasband and contributors, National Institutes of Health, USA).

The measurement of the angles of interest required drawing an axis on the aforementioned carpal bones. The lunate axis corresponds to the line perpendicular to a line which connects the two distal poles of the lunate, the scaphoid axis corresponds to the line that connects the proximal and distal volar convexities of the scaphoid, and the capitate axis corresponds to the line that connects the center of its distal articular surface to the center of the proximal articular surface [34]. The radial axis was drawn through the center of the radius. The measurement method consisted of obtaining the angles between these axes and a horizontal line (0º) and utilizing these angles to obtain the angles of interest [22]. The described method is shown in Figure 2.11. From the lateral view , the RL angle was calculated by deducting the lunate angle from the radius angle, the SL angle was calculated by deducting the scaphoid angle from the lunate angle, and the CL angle was calculated by deducting the lunate angle from the capitate angle. From the postero-anterior view the RC angle was calculated by deducting the radius angle from the capitate angle.

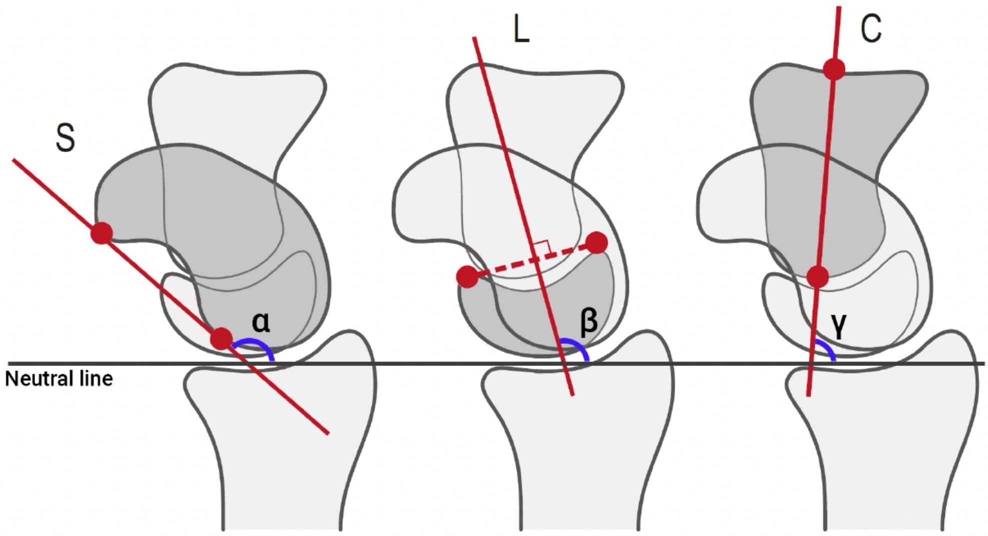

Figure 2.11: Angles measurement method. (S) Scaphoid axis. (L) Lunate axis. (C) Capitate axis. (α) Scaphoid angle. (β) Lunate Angle. (γ) Capitate Angle [22].

Data was gathered and organized in Microsoft Excel (Version 16.61.1, Microsoft, Albuquerque, New Mexico, USA). Microsoft excel was also used for statistical analysis. To assess the significance of the results and understand whether wrist kinematics changed statistically significantly with respect to the shape variation of interest, *e.g.*, mode 1 + 3SD vs. mode 1 -3SD, a two-sample t-test was performed for each shape mode tested. A two-sample t test compares the difference in the means of the same variable between two groups [35]. The t test results in a p-value, between 0 and 1, that states the probability of the difference in results occurring by chance, a p-value lower or equal to 0.05 being considered statistically significant.

3
Results

This chapter describes the accuracy assessment of the lunate implant design, the final updates to the motion guide device, and the results of the experiments on embalmed human specimens. The accuracy test on the implant design and updates to the motion guide device are first described in Section 3.1. The experimental results are presented in Section 3.2.

3.1. Design

3.1.1. Parametric Lunate Implant Design

After designing a parametric lunate implant, described in the previous chapter, it was important to assess how much the designed implant differed from the lunate shape described by the SSM. The accuracy of the implant, compared to the SSM shape, was tested using the mean shape, as it is the shape used as a template for the design. A body comparison was performed in Solidworks, showing in blue the areas of the design that deviate outwards and in yellow/red the areas that deviate inwards. An image of the body comparison is shown in Figure 3.1.

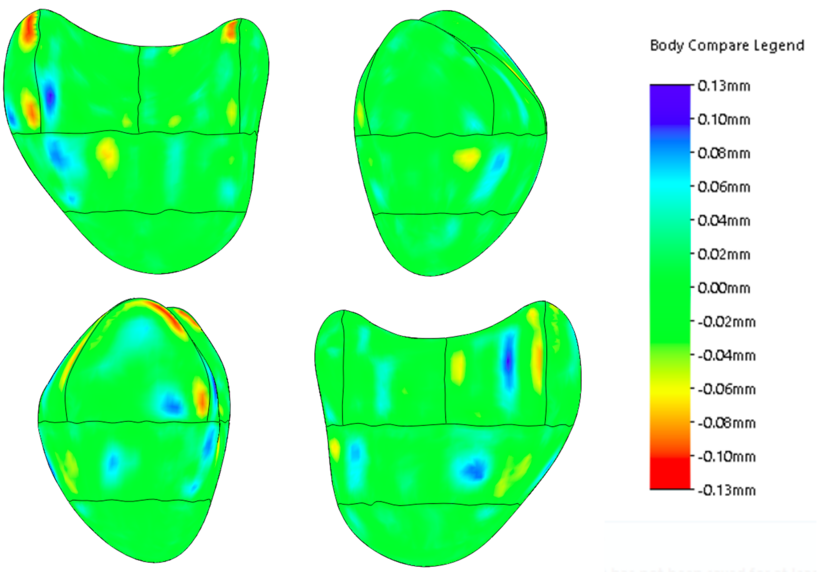

Figure 3.1: Images of the mean lunate implant design when compared with the original SSM shape.

The analysis showed that there is a slight deviation in some areas of the design, in particular on the two distal poles of the lunate and around the central area. The deviations are shown to range between 0.00 and 0.13 millimeters, either inward or outward.

3.1.2. Handheld Motion Guide Device Updates

After previous evaluations of the handheld motion guide device, two requirements were established to solve the encountered issues. The timing belts were to be tensioned and aligned, and the pulley plastic screws were to stay straight throughout the usage of the device in order for the device to move as expected. Therefore, it was necessary to find a way to modify the device to meet these requirements.

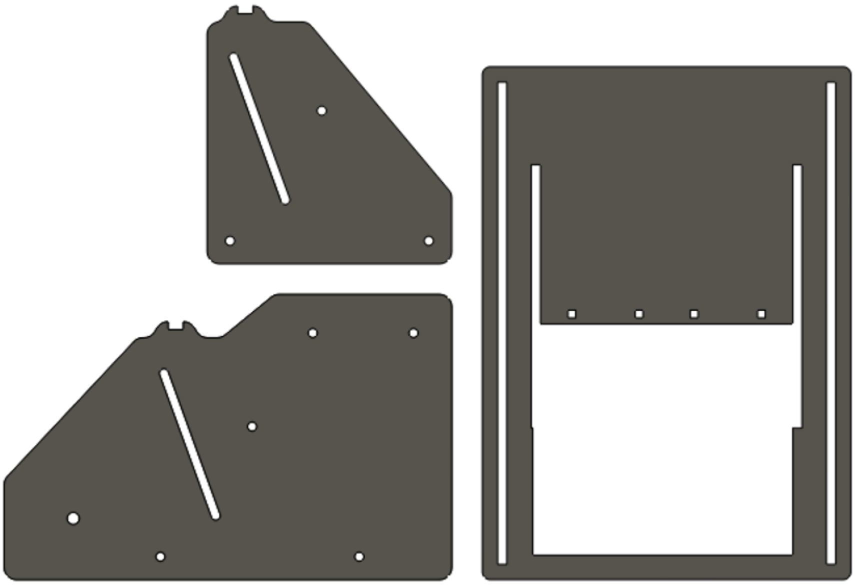

Figure 3.2: Designed side plates (left) and bottom plate (right) used to update the handheld device.

To solve the problems, multiple parts were designed and implemented in the previous design. In order to ensure that the pulley screws were straight and did not bend while the device is used, a side plate was designed and implemented on either side of the device. The side plates were designed with holes through which the screws fit, providing support and preventing bending. In addition, a smaller side plate was designed to, in combination with the larger plate, hold a belt tensioner and ensure the pulley belts would not get loose. Both side plates were fitted with three purposely placed holes that are used to fix the two plates with spacers. A screw slot was also fitted to hold the belt tensioner in different positions and a notch was placed on the top to hold an elastic in a fixed position. A bottom plate was also designed to fit the whole device and prevent the plates from moving. The two side plates and the bottom plate are shown in Figure 3.2. CAD drawings of the updated handheld device are shown in Figure 3.3, comparing the new updated version with the previous design. The added parts are represented in blue for easier identification of the updates.

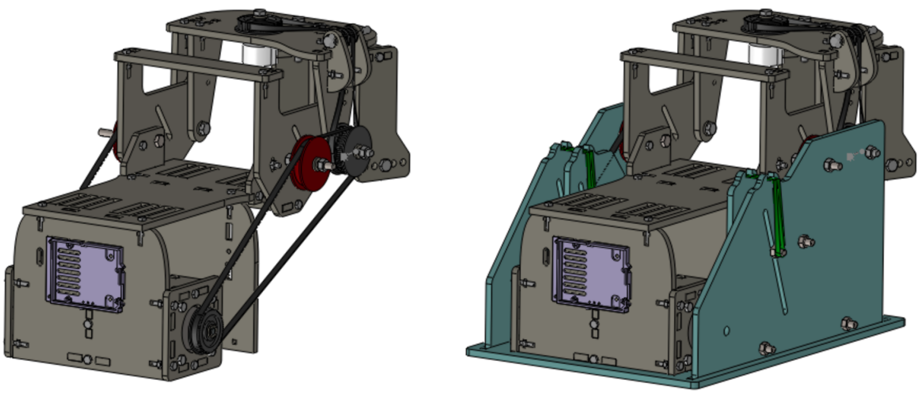

Figure 3.3: CAD drawings of the previous iteration of the handheld device (left) and the updated version (right). The added parts are represented in blue.

All the plates were laser-cut out of 8mm transparent PMMA, similar to the majority of the device, making it easier to clean and improving visibility of the hand and arm. The spacers and belt tensioners were 3D-printed in white PLA filament. The screws and nuts used were made of nylon. Since the apparent issues were design related, no updates were made to either the drive system or the electronics of the device. A picture of the final design is shown in Figure 3.4.

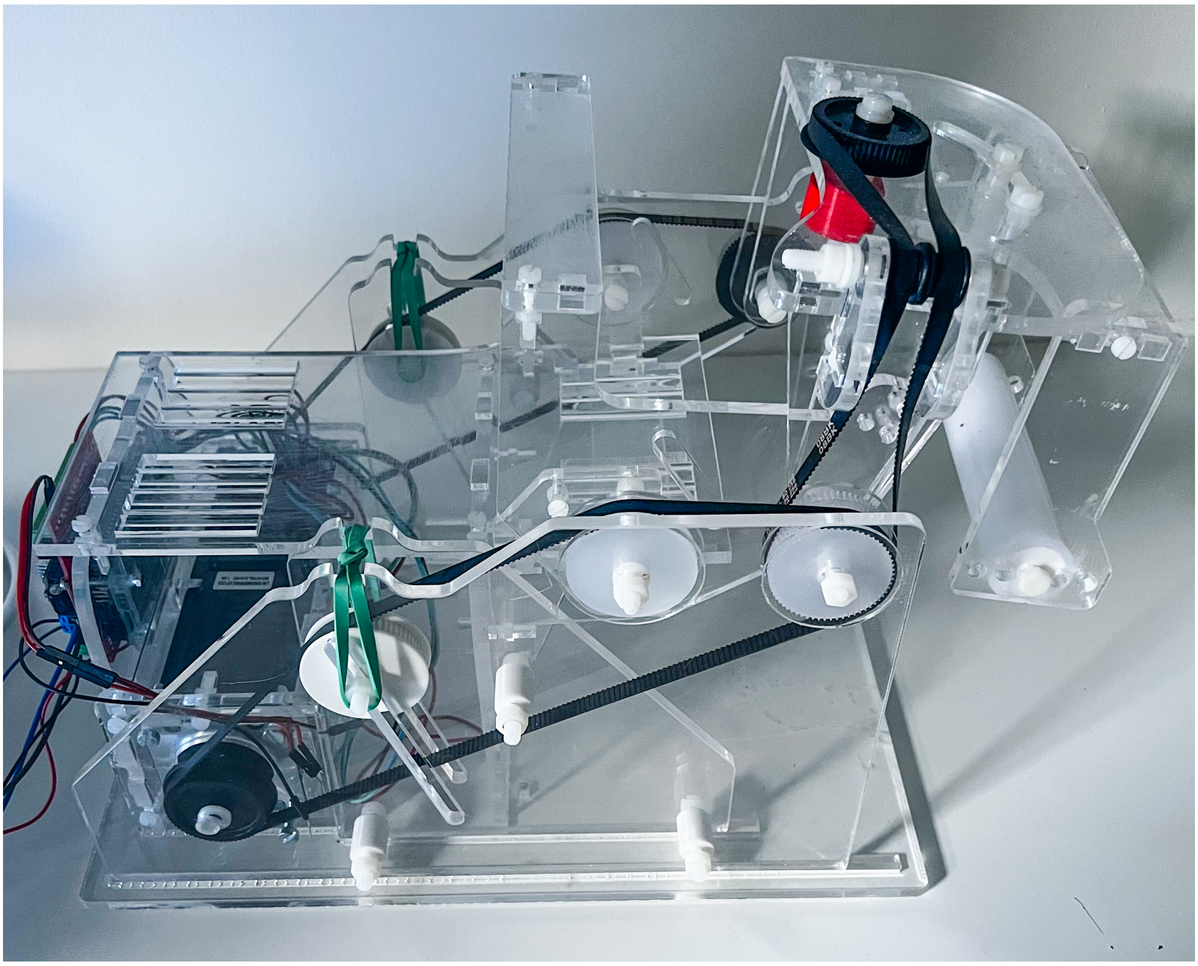

Figure 3.4: Final iteration of the Handheld Motion Guide Device.

3.2. Experiment

The experiment resulted in a total of 84 tests, 42 per specimen. The scapholunate, capitolunate, and radiolunate mean angles were calculated for each FE test using the method described in Section 2.3. and are shown in Figures 3.5-7. The calculated scapholunate, capitolunate, and radiolunate angles with healthy lunates were, respectively, 71.25º, 14.45º, and 22.91º for specimen 1 and 73.25º, 33.71º, and 31.40º for specimen 2. The FE tests show a generalized increase in scapholunate and capitolunate angle when using implants when compared with the original healthy lunate. The healthy lunate scans of the same specimens were previously taken by a different student before updating the handheld device and before the scapholunate ligaments (SLIL) and lunotriquetral ligaments (LTIL) were transected. The RUD tests were not included in the results since the device did not work properly, as it does not perform the full range of motion in the radial direction and little to no motion in the ulnar direction.

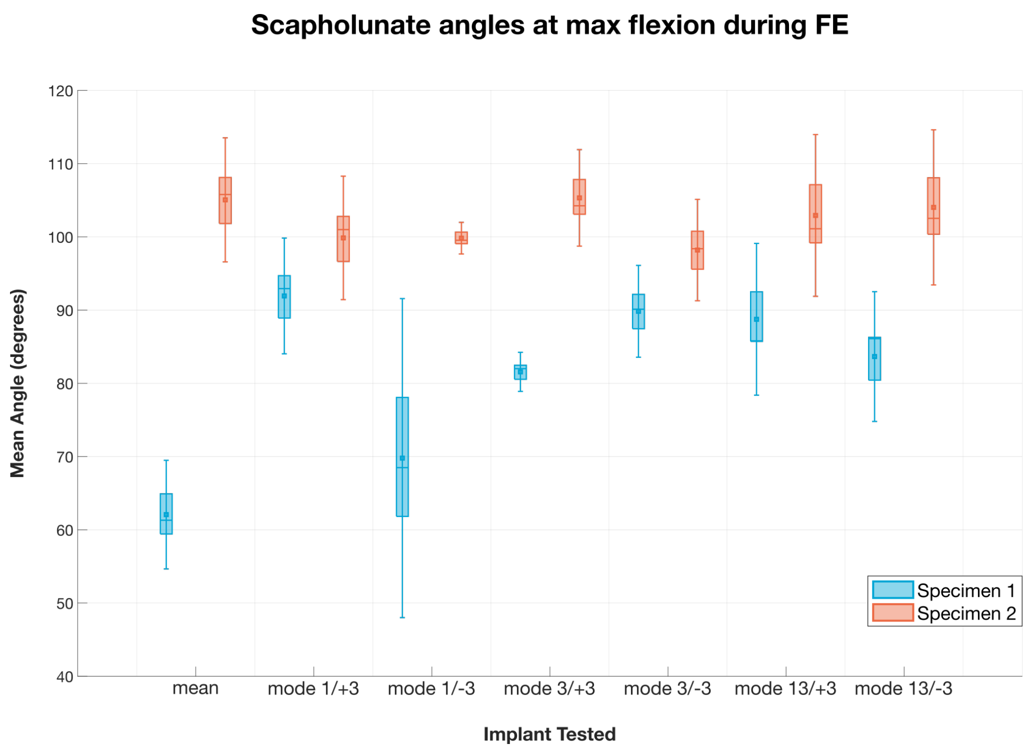

Figure 3.5: Box plots with the distribution of scapholunate angles at max flexion during FE tests of specimen 1 (blue) and specimen 2 (orange). Scapholunate angles with the healthy lunate were 71.25º and 73.25º, for specimen 1 and 2, respectively. Error Bars represent +/- 2SD. The mean is represented with a circle on each box.

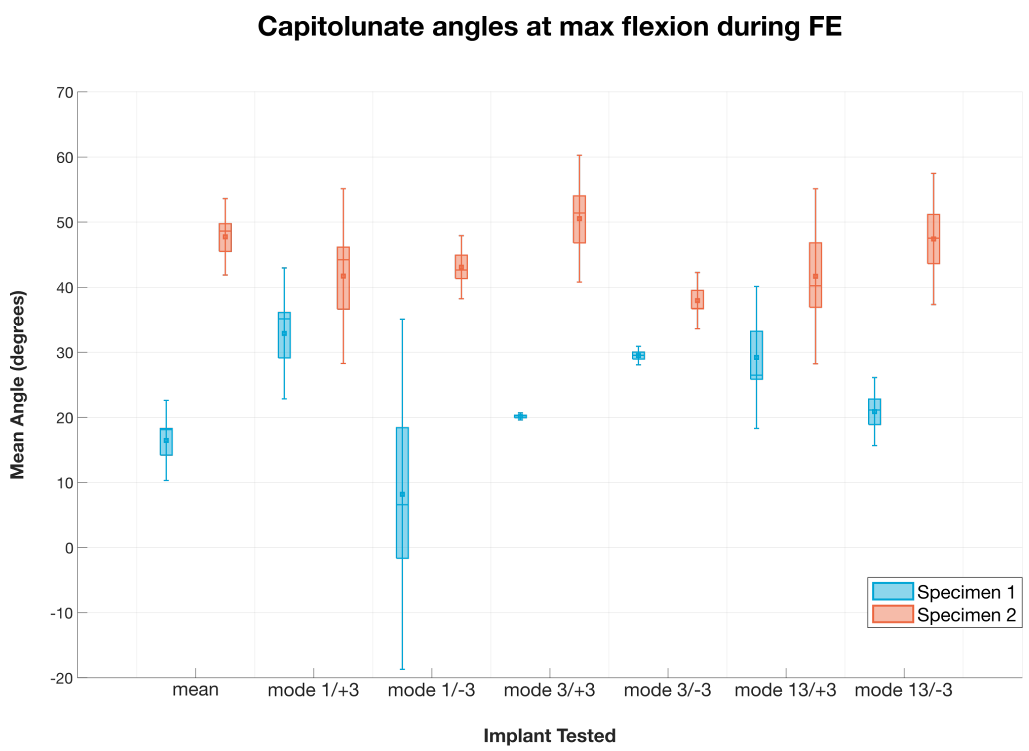

Figure 3.6: Box plots with the distribution of capitolunate angles at max flexion during FE tests of specimen 1 (blue) and specimen 2 (orange). Capitolunate angles with the healthy lunate were 14.45º and 33.71º, for specimen 1 and 2, respectively. Error Bars represent +/- 2SD. The mean is represented with a circle on each box.

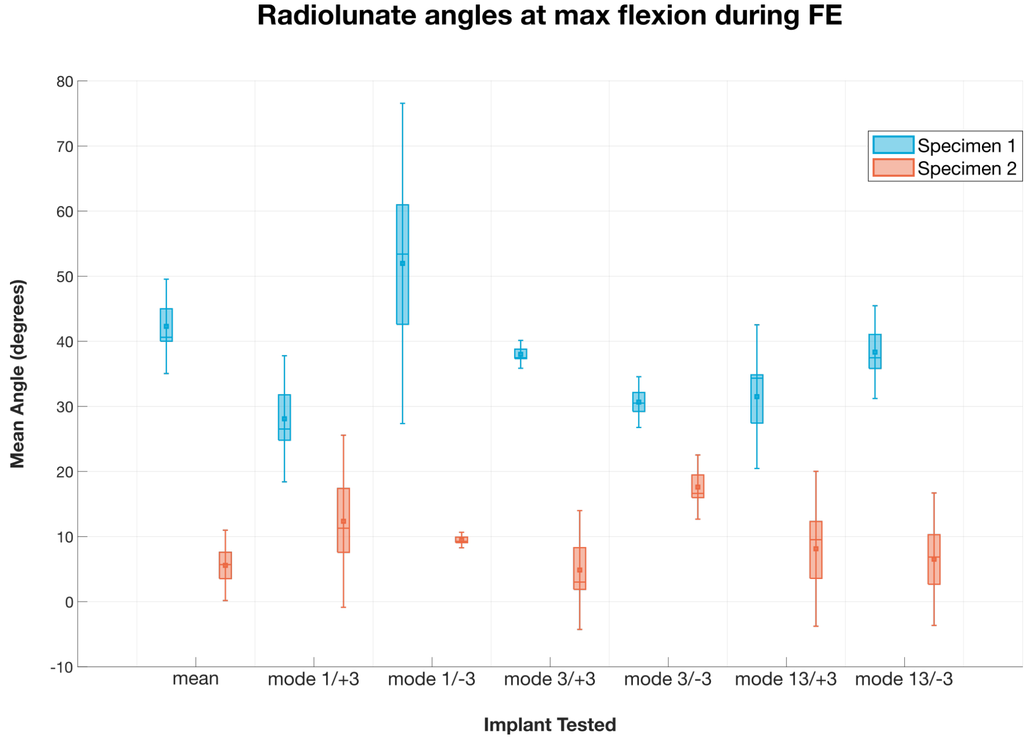

Figure 3.7: Box plots with the distribution of radiolunate angles at max flexion during FE tests of specimen 1 (blue) and specimen 2 (orange). Radiolunate angles with the healthy lunate were 22.91º and 31.40º, for specimen 1 and 2, respectively. Error Bars represent +/- 2SD. The mean is represented with a circle on each box.

A two-sample t test was performed between the results of each two different implant designs tested for each mode. The results are shown in Tables 3.1-3. The results show that mode 3 has a significant effect on the measured angles, with a p-value (two-tailed) smaller than 0.05 in 5 of the 6 t-tests performed and only one having a p-value larger than 0.05 (i.e., 0.06). The values obtained for the other modes show that their effect is not statistically significant, with only one test in mode 1 having a p-value lower than 0.05. In the meantime, it is of note that tests with mode 1 and 13 have much larger variance discrepancies, which also affect the t-test results.

Table 3.1: Two-Sample t test results for scapholunate angle. P-values smaller than 0.05 are highlighted in green.

	Mode 1				**Mode 3**				**Mode 13**			
	Specimen 1		**Specimen 2**		**Specimen 1**		**Specimen 2**		**Specimen 1**		**Specimen 2**	
	+3SD	**-3SD**	**+3SD**	**-3SD**	**+3SD**	**-3SD**	**+3SD**	**-3SD**	**+3SD**	**-3SD**	**+3SD**	**-3SD**
Mean	91,933	69,788	99,858	99,820	81,566	89,837	105,326	98,198	88,744	83,659	102,926	104,028
Variance	15,612	118,582	17,770	1,166	1,777	9,833	10,851	11,970	26,840	19,616	30,492	28,042
p-value	0,046		0,989		0,025		0,061		0,266		0,815	

Table 3.2: Two-Sample t test results for capitolunate angle. P-values smaller than 0.05 are highlighted in green.

	Mode 1				Mode 3				Mode 13			
	Specimen 1		Specimen 2		Specimen 1		Specimen 2		Specimen 1		Specimen 2	
	+3SD	-3SD	+3SD	-3SD	+3SD	-3SD	+3SD	-3SD	+3SD	-3SD	+3SD	-3SD
Mean	32,899	8,185	41,704	43,071	20,151	29,499	50,526	37,942	29,211	20,889	41,679	47,408
Variance	25,273	180,732	45,042	5,865	0,073	0,505	23,719	4,646	29,722	6,819	45,173	25,368
p-value	0,058		0,762		0,0002		0,026		0,097		0,303	

Table 3.3: Two-Sample t test results for radiolunate angle. P-values smaller than 0.05 are highlighted in green.

	Mode 1				Mode 3				Mode 13			
	Specimen 1		Specimen 2		Specimen 1		Specimen 2		Specimen 1		Specimen 2	
	+3SD	-3SD	+3SD	-3SD	+3SD	-3SD	+3SD	-3SD	+3SD	-3SD	+3SD	-3SD
Mean	28,093	51,964	12,351	9,468	37,998	30,658	4,862	17,604	31,496	38,334	8,124	6,524
Variance	23,460	151,262	43,671	0,353	1,145	3,794	20,827	6,075	30,443	12,706	35,389	25,868
p-value	0,052		0,530		0,011		0,024		0,169		0,741	

4 Discussion

This chapter analyzes and discusses the results of the lunate implant design, the final updates to the motion guide device, and the experiments on embalmed human specimens, presented in Chapter 3, and provides recommendations for future studies. The limitations of this study are also discussed in this chapter, followed by a conclusion.

4.1. Implant Design

The implant design method translated the shapes described by the SSM into a surface-based model, using a reduced number of points. Automating the implant design process was possible, reducing the time required to obtain the desired lunate shapes. However, some issues were encountered.

As shown in the previous chapter, the implants lack accuracy in some areas, with a maximum deviation of around 0.13 millimeters when analyzing the mean shape. However, compared to other studies that evaluate the precision of the approximate shape of a carpal bone with its original shape, our lunate implant design has high accuracy, a study by Eschweiler showing a larger maximum deviation of 0.28 mm when comparing two trapezium shapes (original vs. morphed approximation) still being considered highly accurate [36].

Although there will always be small deviations when the number of points used is reduced, it is important to understand the reason for these deviations. One of the reasons why this happens is because of the CAD software surface tools and how it creates surfaces out of the splines. In some instances, the surface does not strictly follow the splines used in its creation, leading to inaccuracies in shape. An example of this can be seen in Figure 4.1. A reason for this is the irregular shape of the splines, as the points of each spline are no longer in the same plane when they are created using the SSM coordinate points (see Figure 2.6), which requires the software to generate a surface out of splines with more complex shapes. The approximated loft technique, used in both the boundary surface and filled surface commands, approximates the surface shape to the contours of the splines, being more difficult to obtain sufficient accuracy with more complex shapes [19]. Reducing the amount of points, making the shapes more simple, might not accurately describe the shape of the lunate but allow a closer surface approximation, while increasing the number of points leads splines that more accurately depict the lunate shape but causes difficulties in surface creation due to the complexity of the shapes. Finding the balance between these two aspects proved to be the most challenging aspect of this method.

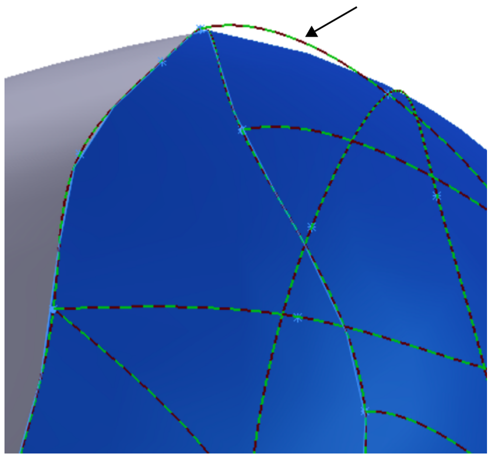

Figure 4.1: Surface does not follow the contour of a spline on one of the distal poles of the lunate (an arrow points at the spline).

Another issue encountered with the design is that in some cases the surfaces cannot be knit into a solid model. This is once again caused by the inability of the software to strictly follow the contours of the splines, in this case the boundary splines. Although the same spline is used on surfaces bounded to each other, some resulting surfaces have inaccuracies in the shape of their boundaries, and since the Surface Knit command has a maximum knitting tolerance of 0.1 millimeters, any gap larger than that makes it impossible to knit the surfaces [37]. There are also cases where the surfaces can be knit but it cannot create a solid body with the surface knit command. In that case, the thicken command can be used to transform the knitted surfaces into a solid body [38].

Although the implant design shows high accuracy compared to literature, we do not know how the design inaccuracies affect its performance once implanted. It is, therefore, important to fix these issues and improve the overall design. To improve the implant design in future studies, it would be encouraged find a way to maintain the points for each spline on the same plane when matching point from the SSM to the points used in the preliminary design. Making the splines straight, when looking at them from one plane, would decrease the complexity of said shapes and possibly increase the accuracy of surface generation, also reducing the possibility of gaps between adjacent surfaces. The SSM points are dispersed on a point cloud, making it improbable for the nearest points to be in the same plane, specially when applying the design to different modes. However, it might be the case that modifying the coordinates of said points to be in the same plane, while not matching any point in the SSM, would lead to an overall shape that more accurately depicts the lunate shapes described by the SSM.

4.2. Handheld device updates

When analyzing the changes made to the handheld device and how the device performs compared to previous tests, it can be concluded that the performance of the device has improved. The addition of side plates to the original design was successful in stopping the nylon screws from bending during the motions tested, at the same time resulting in a much more stable and sturdy construction. This was assessed by performing a couple of tests with the specimens, prior to the official ones with the CT scanner. Furthermore, the incorporation of a belt tensioner on the side plates ensured that the side belts were tensioned throughout the experiment. All of these changes resulted in the device working as expected during the FE movements, solving the issues encountered in previous tests.

Meanwhile, despite multiple improvements, the device did not work as intended during RUD motions. While it works well by itself, it performs poorly with the added weight of a sample, not doing the intended motion. This happens because of the way the RUD mechanism is designed. Firstly, while the main timing belt, responsible for that movement, was tensioned, the twisted belt on the top was not, possibly resulting in failure to transfer energy from one belt to the other. Furthermore, a looser belt is likely to skip teeth in the gears or even fall off the gears, leading to problems with the belt chain [39, 40]. Lastly, the twisted belt on the top is misaligned, which can lead to increased wear on the side surfaces of the belt and uneven belt tension [39, 40].

To improve the transfer of energy from one belt to the other, better gearing could be introduced, using a stronger material than plastic. Moreover, a modification to make the piece that twists the belt responsible for the RUD movement sit at a leveled position could improve its tensioning and improve its alignment. If these recommendations do not work, however, it may be necessary to look into a different belt mechanism for the RUD movement. It is of note that the experimental situation in which the device is used to force movement on an embalmed human specimen differs from the real-life situation in which the wrist is actively moved by a patient. At this stage, however, it is not possible do perform this type of tests in vivo.

When looking at the usability of the device, there are other improvements that could be made. One area that could be improved is wire management. The motors used are appropriate for the application, but its wires are exposed to the environment. The wires must be covered during experiments to prevent them from getting wet, which is not a long-term solution. The same can be said about the Arduino board, whose wires are not only exposed but also easy to disconnect with any accidental movement. This could be solved with a compartment that houses the wires and the Arduino board in a way that only the buttons are exposed. While these are not vital changes for the performance of the device, these would improve its usability.

4.3. Experiment and effects of lunate shape on wrist kinematics

The effect of the lunate implant shape on wrist kinematics was evaluated by comparing the scapholunate, capitolunate, and radiolunate angles. When comparing the measurements taken with the lunate implants with those taken with the original lunate bones, there is an increase in the scapholunate and capitolunate angles, although the capitolunate angles are presented as negative because of the way they are measured. Considering that the scans taken of the original lunates were taken before the interosseous ligaments were severed, the observed angle changes are expected. Clinical data and expertise shows that there is an increase in scaphoid flexion during FE motion when interosseous ligaments are sectioned, the scapholunate ligament (SLIL) in particular [41]. The SLIL is the primary stabilizing ligament of the scapholunate articulation, and its severing is directly associated with scapholunate advanced collapse (SLAC) [42]. SLAC been shown to lead to rotary subluxation of the scaphoid, which in practice leads to an increase in the angle of the scapholunate, consequently affecting the kinematics of the wrist. The capitolunate joint is also affected by SLAC, leading to proximal migration of the capitate and ulnar displacement of the lunate [42].

The two-sample t tests showed mode 3's effect on the measured angles to be significant on both specimens tested. For specimen 1, there was a statistically significant difference between the implant with +3 SD and the one with -3 SD for the three measured angles, SL, CL, and RL, while for specimen 2 there was a statistically significant difference for the CL and RL angles. When it comes to the SL angle, mode 3 having a significant effect can be explained. Of the three modes tested, mode 3 is the one that represents a shape variation that directly described the angle between the radial side, which articulates with the scaphoid, and the proximal side, that articulates with the radius on the volar side. The change described by mode 3 affects the joint relation between the scaphoid and the lunate. While there was a significant effect, it is hard to stipulate how it affects the kinematics of the wrist, since the change in SL, RL, and CL angles is different when comparing specimen 1 and 2. A significant effect by the other two modes was hypothesized, but the results of our experiment refute this hypothesis. Mode 1 was thought to generate a significant effect on wrist kinematics based on the fact that it has the highest contribution to shape variation out of all modes and because it aligns with previously described D, V, and N-type lunates, with higher, lower, and equal heights of the dorsal and volar sides, respectively [14]. In this study, the implants for mode 1 with +3SD and -3SD correspond to type D- and V-, respectively. These two types of lunates were shown in a previous study by Watson to have a statistically significant difference in radiolunate angle [24]. However, that was not observed in this study. Mode 13, on the other hand, describes a variation that is in line with Viegas' classification of V-Type I or II lunates, which is characterized by the addition of a medial facet for articulation with the hamate [43]. In this study, the implants for mode 13 with +3SD and -3SD correspond to type II and type I, respectively. This shape variation was clinically shown to affect the kinematics of the wrist, type I lunates exhibiting more translation during radial deviation and type II lunates displaying more flexion during radial deviation of the wrist, the addition of a medial facet forcing the wrist to act in an extension and flexion plane and minimizing rotation and translation [43]. Similarly, a different study showed increased radiocarpal motion in wrists with type II lunates during flexion-extension [30]. Therefore, a difference in wrist kinematics was expected during both the FE and RUD motions. However, this was not observed on the results from tests performing the FE motion and the tests performing the RUD motion had to be excluded from this study, as the device did not work properly.

The difference in results between repeated tests is a possible reason for the results of modes 1 and 13 not being statistically significant. Looking at the results, even though not in all tests, repeatability of the same test does not produce the same results. There is high variability in results obtained with the same test, with great difference in standard deviation when comparing different modes tested, *e.g.*, tests on specimen 1 with implants representing shape mode 1 +3SD and -3SD have standard deviations of 5.027º and 13.444º respectively. Standard deviations are higher with smaller sample sizes, and in this study only 3 tests were performed per implant. When samples have high standard deviations, it is particularly difficult to attribute a statistically significant difference between the means because the sampling variability obscures the difference, which may have been the cause of the statistical analysis results [44]. Moreover, it is possible that the lunate implants, given that these do not have ligamentous connections and have free movement, move or shift position in between tests, causing such different results with repeated tests. Future evaluations of wrist kinematics with lunate implants should focus on maintaining or recreating the interosseous ligament connections of the carpal bones. Future lunate implants should implement artificial ligaments in the design, creating a hard-soft tissue interface that recreates the severed ligaments during the excision of the original lunate, as the loss of these ligaments leave the wrist with instability and improper carpal motion.

Another issue that may affect the measurements is the visibility of the lunate implants on CT Scans. The implants were 3D printed using an SLA 3D printer using an engineering resin that resulted in parts with a smooth surface finish, good mechanical properties, and compatible for use in CT scanning. However, the visibility of the implants is poor, causing difficulty to differentiate between the implant and surrounding soft tissue (see Figure 4.2). The difficulty to see the contours of the implant increases the possibility for errors during the measurements, decreasing the reliability of the results. To fix this, there is a possibility to adjust the CT settings in which tissue can be better visualized but at the expense of bone setting. Also, the use of an MRI would provide better images, but these have increased costs and require more time when compared to CT scans, making it unusable in this experiment [45]. On the other hand, a material that is more visible in CT scans could also be used in future studies. A material that has a density closer to that of bone will make the contours of the implant more visible on CT scans. It is of note that these are trial implants with no biocompatibility concern, so the material used should also be affordable and easy to manufacture.

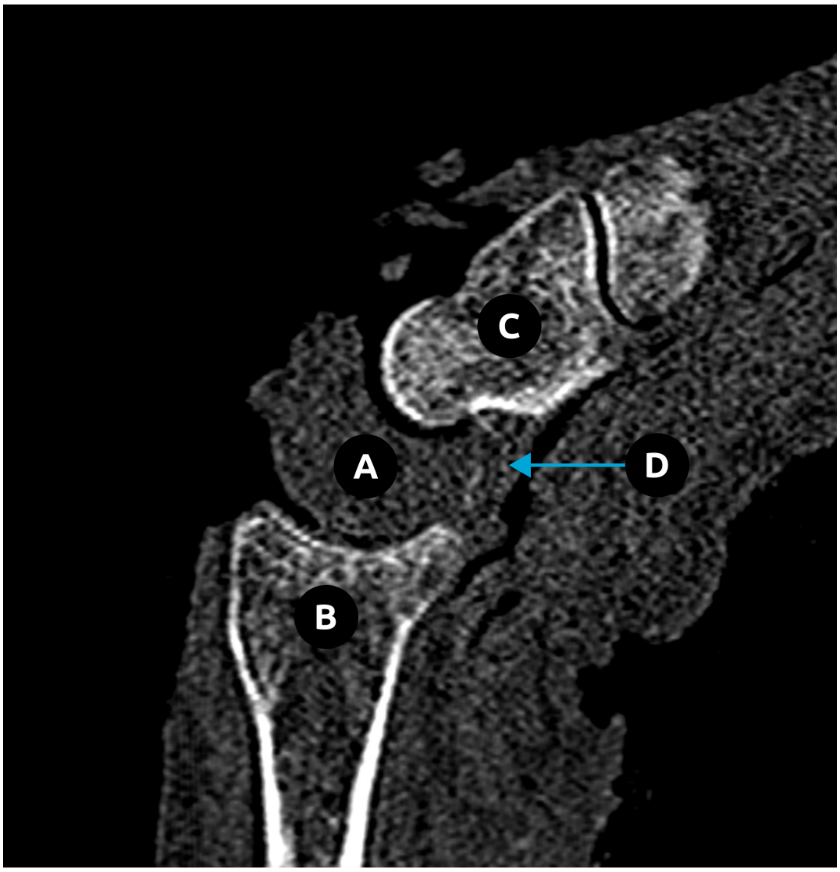

Figure 4.2: Scan of specimen 1 with lunate implant during flexion. A) Lunate Bone. B) Radius Bone. C) Capitate Bone. D) Zone with low visibility of the contours of the lunate implant.

4.4. Limitations

This study has several limitations. Due to time limitations, measurements were taken by only one person, therefore, inter-observer reliability could not be assessed.

Another limitation is that only two specimens were tested, with a repeatability of 3 per test. Using a larger sample and more tests, as previously explained, would provide a better statistical value with a smaller standard deviation, ensuring a more reliable statistical analysis. It is also impossible to compare the results from the implants tested with the original shape since they don't have the same conditions in terms of preserved ligaments, operator, and iteration of the device.

Lastly, the improper functioning of the device when performing the RUD motion prevents one from drawing conclusions from these tests. The RUD motion is an important movement of the wrist and would provide information about the effect of lunate morphology that FE motion alone cannot provide.

4.5. Conclusion

In this research a method to design a patient specific lunate implant was developed and the effect of various lunate shape variations on wrist kinematics was evaluated, using an updated handheld motorized motion guidance device and a 4D CT scanner. The lunate implant design was successful in obtaining the desired shapes described by the statistical shape model, and automatizing the design process proved useful in reducing the time and labor to obtain different lunate shapes. The updated handheld device was successful in performing the FE motion during 4D CT scans, albeit inconsistent during RUD motion. The 4D CT scans produced while using the motion device were usable for analysis, but the 3D printing material used on the lunate implants caused some issues in visibility, though it was still possible to get all the measurements. Meanwhile, testing using different lunate shapes provided important data for understanding the effect of lunate morphology on the wrist kinematics.

This study shows that a statistical shape modeling approach is feasible in designing a parametric lunate implant. It can also be said that lunate shape variations have an effect on wrist kinematics, concluded from the fact that the shape variation described by mode 3 was considered statistically significant to the kinematics of the wrist. However, the difference observed between the tests performed with implants and those on wrists with healthy lunates led us to understand that some form of ligament fixation of the implant would be required to approach the native wrist kinematics with a lunate implant.

References

[1] K.Lutsky and P.K. Beredjiklian. "Kienböck disease". In: *Journal of Hand Surgery* 37.9 (2012), pp. 1942–1952. URL: https://doi.org/10.1016/j.jhsa.2012.06.029.

[2] D. Cross and K.S. Matullo. "Kienböck disease". In: *Orthopedic Clinics of North America* 45.1 (2014), pp. 141–152. URL: https://doi.org/10.1016/j.ocl.2013.09.004.

[3] Y. Kijima and S.F. Viegas. "Wrist Anatomy and Biomechanics". In: *Journal of Hand Surgery* 34.8 (2009), pp. 1555–1563. URL: https://doi.org/10.1016/j.jhsa.2009.07.019.

[4] J.J. Crisco M.J. Rainbow A.L. Wolff and S. W. Wolfe. "Functional kinematics of the wrist". In: *Journal of Hand Surgery* 41.1 (2016), pp. 7–21. URL: https://doi.org/10.1177/1753193415616939.

[5] J. Eschweiler et al. "Anatomy,Biomechanics, and Loads of the Wrist Joint". In: *Life* 12.188 (2022), pp. 1–17. URL: https://doi.org/10.3390/%20life12020188.

[6] G. Bain et al. "The Etiology and Pathogenesis of Kienböck Disease". In: *Journal of Wrist Surgery* 5.4 (2016), pp. 248–254. URL: https://doi.org/10.1055/s-0036-1583755.

[7] D. Rioux-Forker and A.Y. Shin. "Osteonecrosis of the Lunate: Kienböck Disease". In: *The Journal of the American Academy of Orthopaedic Surgeons* 28.14 (2020), pp. 570–584. URL: https://doi.org/10.5435/JAAOS-D-20-00020.

[8] C.M.K. Kalu G.P. Kolovich and M.E. Ruff. "Current Trends in Treatment of Kienböck Disease". In: *Hand* 11.1 (2016), pp. 113–118. URL: https://doi.org/10.1177/1558944715616953.

[9] C.M. Steyers and W.F. Blair. "Measuring ulnar variance: A comparison of techniques". In: *Journal of Hand Surgery* 14.4 (1989), pp. 607–612. URL: https://doi.org/10.1016/0363-5023(89)90175-5.

[10] T. Viljakka et al. "Long-Term Clinical Outcome After Titanium Lunate Arthroplasty for Kienböck Disease". In: *Journal of Hand Surgery* 43.11 (2018), 945e.1–945e.10. URL: https://doi.org/10.1016/j.jhsa.2018.02.009.

[11] D. Egloff et al. "Silastic Implants of the Scaphoid and Lunate: A long-term clinical study with a mean follow-up of 13 years". In: *Journal of Hand Surgery* 18B.6 (1993), pp. 687–692.

[12] T. Viljakka et al. "Long-term outcome (22-36 years) of silicone lunate arthroplasty for Kienböck's disease". In: *Journal of Hand Surgery* 39.4 (2014), pp. 405–415. URL: https://doi.org/10.1177/1753193413489460.

[13] N.J. Visser et al. "Lunate implant arthroplasty: analysis of physical function and patient satisfaction". In: *European Journal of Plastic Surgery* 40.3 (2017), pp. 229–234. URL: https://doi.org/110.1007/s00238-016-1248-9.

[14] N.Tümer et al. "The three-dimensional shape symmetry of the lunate and its implications". In: *Journal of Hand Surgery* 46.6 (2021), pp. 587–593. URL: https://doi.org/10.1177/17531934211004080.

[15] M. Henry. "Outcomes assessment of lunate replacement arthroplasty with intrinsic carpal ligament reconstruction in Kienböck's disease". In: *Hand* 9.3 (2014), pp. 364–369. URL: https://doi.org/10.1007/s11552-014-9624-z.

[16] J. Milovanovic et al. "Designing of patient-specific implant by using subdivision surface shaped on parametrized". In: *Tehnicki Vjesnik* 28.3 (2021), pp. 801–809. URL: https://doi.org/10.17559/TV-20200502215442.

[17] T. Huysmans et al. "Multi-patch B-spline statistical shape models for CAD-compatible digital human modeling". In: *Advances in Intelligent Systems and Computing* (2019), pp. 179–189. URL: https://doi.org/10.1007/978-3-319-94223-0_17.

[18] A.Lowe. *Zen & The Art of Solidworks Surfacing*. https://f64bd4.p3cdn1.secureserver.net/wp-content/uploads/SWW2018_ZenSurfacing.pdf. 2018.

[19] G. Lends et al. "Effectiveness analysis of spline surfaces creating methods for shell structure modelling". In: *Geoinformatica Polonica* 20 (2021), pp. 41–53. URL: https://doi.org/10.4467/21995923GP.21.004.14975.

[20] mathworks.com. *dsearchn*. Feb. 2024. URL: https://nl.mathworks.com/help/matlab/ref/dsearchn.html.

[21] N. Sarkalkan et al. "Statistical shape and appearance models of bones". In: *Bone* 60 (2014), pp. 129–140. URL: https:///dx.doi.org/10.1016/j.bone.2013.12.006.

[22] W.H.A. Crezee. "Development of a motion guidance device for 4D CT scans of the wrist". PhD thesis. Delft University of Technology, 2022.

[23] G. Hogenbool. "Reliability research of a motion guidance device for the wrist". PhD thesis. The Hague University of Applied Sciences, 2023.

[24] H.K. Watson et al. "Lateral lunate morphology: an x-ray study". In: *Journal of Hand Surgery* 21.5 (1996), pp. 759–763. URL: https://doi.org/10.1016/S0363-5023(96)80188-2.

[25] J.M. Antuña Zapico. "Malacia Del Semilunar". PhD thesis. Universidad de Valladolid, 1966.

[26] C. Lamas et al. "The anatomy and vascularity of the lunate: considerations applied to Kienböck's disease". In: *Chirurgie de la Main* 26.1 (2007), pp. 13–20. URL: https://doi.org/10.1016/j.main.2007.01.001.

[27] S.B.M. MacLean et all. "The Pathoanatomy and Biomechanics of Kienbock Disease". In: *Hand Clinics* 38 (2022), pp. 393–403. URL: https://doi.org/10.1016/j.hcl.2022.03.003.

[28] D. Jafari et all. "The Effect of Proximal Lunate Morphology "Zapico Classification" on Kienbock's Disease". In: *Journal of Research in Orthopedic Science* 4.3 (2017), pp. 1–4. URL: https://doi.org/10.5812/soj.123038.

[29] S.F. Viegas et al. "Medial (hamate) facet of the lunate". In: *Journal of Hand Surgery* 15.4 (1990), pp. 564–571. URL: https://doi.org/10.1016/s0363-5023(09)90016-8.

[30] G.I. Bain et al. "The effect of lunate morphology on the 3 dimensional kinematics of the carpus". In: *Journal of Hand Surgery* 40.1 (2015), pp. 81–89. URL: https://doi.org/10.1016/j.jhsa.2014.09.019.

[31] I. Galley et al. "Influence of lunate type on scaphoid kinematics". In: *Journal of Hand Surgery* 32.6 (2007), pp. 842–847. URL: https://doi.org/10.1016/j.jhsa.2007.03.012.

[32] Formlabs. *FDM vs. SLA: Compare Filament and Resin 3D Printers*. Mar. 2024. URL: https://formlabs.com/eu/blog/fdm-vs-sla-compare-types-of-3d-printers/.

[33] J.G.G. Dobbe et al. "Evaluation of a Quantitative Method for Carpal Motion Analysis Using Clinical 3-D and 4-D CT Protocols". In: *IEEE Transactions on Medical Imaging* 38.4 (2019), pp. 1048–1057. URL: https://doi.org/10.1109/TMI.2018.2877503.

[34] S.G. Davies. "Radiography and Arthrography". In: *Imaging of the Hand and Wrist*. Ed. by A.L. Baert et al. Medical Radiology. Diagnostic Imaging, 2013, pp. 1–21.

[35] UCLA: Statistical Consulting Group. *T-Test: Stata Annotated Output*. Feb. 2024. URL: https://stats.oarc.ucla.edu/stata/output/t-test/.

[36] J. Eschweiler et all. "Development of a biomechanical model of the wrist joint for patient-specific model guided surgical therapy planning: Part 1". In: *Proceedings of the Institution of Mechanical Engineers, Part H: Journal of Engineering in Medicine* 230.4 (2016), pp. 310–325. URL: https://doi-org.tudelft.idm.oclc.org/10.1177/0954411916632791.

[37] Dassault Systems. *Knit Surface*. Mar. 2024. URL: https://help.solidworks.com/2022/english/SolidWorks/sldworks/HIDD_DVE_KNIT_SURFACE.htm.

[38] Dassault Systems. *Thicken*. Mar. 2024. URL: https://help.solidworks.com/2021/english/SolidWorks/sldworks/t_thicken_feature.htm.

[39] M. Katic et al. "Measurement of timing belt angle transfer accuracy in angle metrology applications". In: *Results in Engineering* 17 (2023), pp. 1–8. URL: https://doi.org/10.1016/j.rineng.2022.100849.

[40] P. Chiariotti et all. “Exploiting Continuous Scanning Laser Doppler Vibrometry in timing belt dynamic characterisation”. In: *MSSP* 86 (2017), pp. 66–81. URL: `http://dx.doi.org/10.1016/j.ymssp.2016.01.001`.

[41] W.H. Short et all. “Biomechanical Evaluation of Ligamentous Stabilizers of the Scaphoid and Lunate”. In: *The Journal of Hand Surgery* 27.6 (2002), pp. 991–1002. URL: `http://doi:10.1053/jhsu.2002.35878`.

[42] B.T. Tischler et all. “Scapholunate advanced collapse: a pictorial review”. In: *Insights Imaging* 5 (2014), pp. 407–417. URL: `http://doi:10.1007/s13244-014-0337-1`.

[43] R.E. Hein et all. “Association of Lunate Morphology With Progression to Scaphoid Fracture Nonunion”. In: *American Association for Hand Surgery* 17.3 (2022), pp. 452–458. URL: `https://doi.org/10.1177/1558944720937368`.

[44] Portland State University. *Jason Newsom's Stats Notes: "Web Lectures," notes, and handouts on introductory graduate-level statistics*. Feb. 2024. URL: `https://web.pdx.edu/~newsomj/pa551/lecture4.htm`.

[45] Johns Hopkins Medicine. *CT Scan Versus MRI Versus X-Ray: What Type of Imaging Do I Need?* Mar. 2024. URL: `https://www.hopkinsmedicine.org/health/treatment-tests-and-therapies/ct-vs-mri-vs-xray`.

A

Experimental Protocol

1. **Setup**
   (a) Cover the CT table
   (b) Place board on CT table
   (c) Attach all wires of the device correctly
   (d) Place device on board and secure it with tie wraps
2. **Specimen Preparation**
   (a) Place specimen 1 on the device with palmar side holding the bar
   (b) Attach specimen to device with elastic straps
   (c) Surgeon insert lunate implant
   (d) Surgeon close dorsal opening with two stitches
3. **4D CT Scans**
   (a) Place device with specimen on the board in the CT scanner
   (b) Make a 4D CT scan of the wrist performing the flexion / extension (FE) motion
   (c) Check Table A.1.
   (d) Repeat step 3(b) and 3(c) two more times
   (e) Make a 4D CT scan of the wrist performing the radial / ulnar deviation (RUD) motion
   (f) Check Table A.1.
   (g) Repeat step 3(e) and 3(f) two more times
4. **Replace Implant**
   (a) Remove power
   (b) Surgeon remove stitches
   (c) Surgeon remove implant
   (d) Surgeon insert next lunate implant
   (e) Surgeon close dorsal opening with two stitches
   (f) Repeat steps 3 (4D CT Scans) and 4 (Replace Implant) for all implants to be tested on the first specimen.
5. **Replace Specimen**
   (a) Remove power
   (b) Surgeon remove stitches
   (c) Surgeon remove implant
   (d) Detach specimen 1 from device
   (e) Repeat steps 2 (Specimen Preparation), 3 (4D CT Scans), and 4 (Replace Implant) for the second specimen.

6. **End of Experiment**
   (a) Remove power
   (b) Surgeon remove stitches
   (c) Surgeon remove implant
   (d) Detach specimen 2 from device
   (e) Clean device, CT table and CT room
   (f) Copy CT files to external hard drive
   (g) Cover and store specimens
   (h) Store implants

Table A.1: Specimen/Implant Testing Protocol

Specimen	Mode	SD	Test Type	Test	Done?	Notes
1	mean	-	FE	1	☐	
1	mean	-	FE	2	☐	
1	mean	-	FE	3	☐	
1	mean	-	RUD	1	☐	
1	mean	-	RUD	2	☐	
1	mean	-	RUD	3	☐	
1	1	+3	FE	1	☐	
1	1	+3	FE	2	☐	
1	1	+3	FE	3	☐	
1	1	-3	RUD	1	☐	
1	1	-3	RUD	2	☐	
1	1	-3	RUD	3	☐	
1	3	+3	FE	1	☐	
1	3	+3	FE	2	☐	
1	3	+3	FE	3	☐	
1	3	-3	RUD	1	☐	
1	3	-3	RUD	2	☐	
1	3	-3	RUD	3	☐	
1	13	+3	FE	1	☐	
1	13	+3	FE	2	☐	
1	13	+3	FE	3	☐	
1	13	-3	RUD	1	☐	
1	13	-3	RUD	2	☐	
1	13	-3	RUD	3	☐	
2	mean	-	FE	1	☐	
2	mean	-	FE	2	☐	
2	mean	-	FE	3	☐	
2	mean	-	RUD	1	☐	
2	mean	-	RUD	2	☐	
2	mean	-	RUD	3	☐	
2	1	+3	FE	1	☐	
2	1	+3	FE	2	☐	
2	1	+3	FE	3	☐	
2	1	-3	RUD	1	☐	
2	1	-3	RUD	2	☐	

Continued on next page

Table A.1: Specimen/Implant Testing Protocol

Specimen	Mode	SD	Test Type	Test	Done?	Notes
2	1	-3	RUD	3	☐	
2	3	+3	FE	1	☐	
2	3	+3	FE	2	☐	
2	3	+3	FE	3	☐	
2	3	-3	RUD	1	☐	
2	3	-3	RUD	2	☐	
2	3	-3	RUD	3	☐	
2	13	+3	FE	1	☐	
2	13	+3	FE	2	☐	
2	13	+3	FE	3	☐	
2	13	-3	RUD	1	☐	
2	13	-3	RUD	2	☐	
2	13	-3	RUD	3	☐	

B
Matlab Code

```
load('SSM.mat')
load('IDs.mat')
load('fitting_spec.mat')

b_new = zeros (107,1);
b_new(x,1) = y;
% b_new is the eigenvector with shape parameter and standard deviation (SD) for the modes
% x = mode ; y = SD
% use this method to modify mean shape by applying a SD to a particular mode

or

b_new = zeros (107,1);
b_new = fitting_spec(1:13)
b_new(x,1) = b_new(x,1) + y;
% x = mode ; y = SD
% use this method to apply fitting parameters for a particular specimen add a SD to a
    particular mode

coordenates = m + reshape(P*b_new,size(m'))';
% coordenates = 20446x3 matrix with the coordinates of the all the points in used SSM ; m =
    20446x3 matrix with the coordinates of the SSM meanshape ; P describes modes of variation
    ;

total = length(coordenates);
% total = total amount of points used in the SSM model

A = 1:total;
B = A.';
IDallpoints = [B coordenates];
% IDallpoints = 20446x4 matrix with all the point IDs on first collumn and the coordinates on
    other three collumns

IDpoints = IDallpoints(u,:);
% IDpoints = 719x4 matrix with only the points IDs and coordinates used for the design

points = y(:,[2,3,4]);
% points = coordinates of the design points without the IDs for extraction
```

C

Solidworks Macros

C.1. Spline Macro

```

Dim swApp As SldWorks.SldWorks
Dim Part As SldWorks.ModelDoc2
Dim boolstatus As Boolean
Dim longstatus As Long, longwarnings As Long

Sub main()

Set swApp = Application.SldWorks

Set Part = swApp.ActiveDoc
Dim COSMOSWORKSObj As Object
Dim CWAddinCallBackObj As Object
Set CWAddinCallBackObj = swApp.GetAddInObject("CosmosWorks.CosmosWorks")
Set COSMOSWORKSObj = CWAddinCallBackObj.COSMOSWORKS
Dim myModelView As Object
Set myModelView = Part.ActiveView
myModelView.FrameState = swWindowState_e.swWindowMaximized

Part.SketchManager.Insert3DSketch True
Dim pointArray As Variant
Dim points() As Double
ReDim points(0 To 14) As Double
points(0) = 0
points(1) = 1
points(2) = 2
points(3) = 3
points(4) = 4
points(5) = 5
points(6) = 6
points(7) = 7
points(8) = 8
points(9) = 9
points(10) = 10
points(11) = 11
points(12) = 12
points(13) = 13
points(14) = 14
pointArray = points
Dim skSegment As Object
Set skSegment = Part.SketchManager.CreateSpline((pointArray))
Part.SketchManager.InsertSketch True
Set CWAddinCallBackObj = Nothing
Set COSMOSWORKSObj = Nothing

' Creates a 5-point spline. Each 3 "points(number)=number" describe one point

boolstatus = Part.Extension.SelectByID2("3DSketch2", "SKETCH", 0, 0, 0, False, 0, Nothing, 0)
```

```
Part.EditSketch
Part.ClearSelection2 True
boolstatus = Part.Extension.SelectByID2("Point1", "SKETCHPOINT", 0, 0, 0, False, 0, Nothing,
    0)
boolstatus = Part.Extension.SelectByID2("Point62@Points", "EXTSKETCHPOINT", 0, 0, 0, True, 0,
     Nothing, 0)
Part.SketchAddConstraints "sgCOINCIDENT"
Part.ClearSelection2 True
boolstatus = Part.Extension.SelectByID2("Point2", "SKETCHPOINT", 0, 0, 0, False, 0, Nothing,
    0)
boolstatus = Part.Extension.SelectByID2("Point170@Points", "EXTSKETCHPOINT", 0, 0, 0, True,
    0, Nothing, 0)
Part.SketchAddConstraints "sgCOINCIDENT"
Part.ClearSelection2 True
boolstatus = Part.Extension.SelectByID2("Point3", "SKETCHPOINT", 0, 0, 0, False, 0, Nothing,
    0)
boolstatus = Part.Extension.SelectByID2("Point186@Points", "EXTSKETCHPOINT", 0, 0, 0, True,
    0, Nothing, 0)
Part.SketchAddConstraints "sgCOINCIDENT"
Part.ClearSelection2 True
boolstatus = Part.Extension.SelectByID2("Point4", "SKETCHPOINT", 0, 0, 0, False, 0, Nothing,
    0)
boolstatus = Part.Extension.SelectByID2("Point158@Points", "EXTSKETCHPOINT", 0, 0, 0, True,
    0, Nothing, 0)
Part.SketchAddConstraints "sgCOINCIDENT"
Part.ClearSelection2 True
boolstatus = Part.Extension.SelectByID2("Point5", "SKETCHPOINT", 0, 0, 0, False, 0, Nothing,
    0)
boolstatus = Part.Extension.SelectByID2("Point187@Points", "EXTSKETCHPOINT", 0, 0, 0, True,
    0, Nothing, 0)
Part.SketchAddConstraints "sgCOINCIDENT"
Part.ClearSelection2 True

' Makes each point of the splice coincident to an imported SSM point in a determined order

boolstatus = Part.Extension.SelectByID2("3DSketch2", "SKETCH", 0, 0, 0, False, 0, Nothing, 0)
Part.EditSketch
boolstatus = Part.Extension.SelectByID2("Spline1", "SKETCHSEGMENT", 0, 0, 0, False, 0,
    Nothing, 0)
boolstatus = Part.Extension.SelectByID2("Spline1@3DSketch1", "EXTSKETCHSEGMENT", 0, 0, 0,
    True, 0, Nothing, 0)
Part.SketchAddConstraints "sgTANGENT"
Part.ClearSelection2 True
Part.SketchManager.InsertSketch True

' Makes sure the spline is tangent to any other spline necessary

End Sub
```

C.2. Surface Macro

```

Dim swApp As Object

Dim Part As Object
Dim boolstatus As Boolean
Dim longstatus As Long, longwarnings As Long

Sub main()

Set swApp = Application.SldWorks

Set Part = swApp.ActiveDoc
Dim COSMOSWORKSObj As Object
Dim CWAddinCallBackObj As Object
Set CWAddinCallBackObj = swApp.GetAddInObject("CosmosWorks.CosmosWorks")
Set COSMOSWORKSObj = CWAddinCallBackObj.COSMOSWORKS
Dim myModelView As Object
Set myModelView = Part.ActiveView
```

```
myModelView.FrameState = swWindowState_e.swWindowMaximized

boolstatus = Part.Extension.SelectByID2("3DSketch2", "SKETCH", 0, 0, 0, True, 0, Nothing, 0)
boolstatus = Part.Extension.SelectByID2("3DSketch6", "SKETCH", 0, 0, 0, True, 0, Nothing, 0)
boolstatus = Part.Extension.SelectByID2("3DSketch7", "SKETCH", 0, 0, 0, True, 0, Nothing, 0)
boolstatus = Part.Extension.SelectByID2("3DSketch8", "SKETCH", 0, 0, 0, True, 0, Nothing, 0)
boolstatus = Part.Extension.SelectByID2("3DSketch9", "SKETCH", 0, 0, 0, True, 0, Nothing, 0)

boolstatus = Part.Extension.SelectByID2("3DSketch26", "SKETCH", 0, 0, 0, True, 0, Nothing, 0)
boolstatus = Part.Extension.SelectByID2("3DSketch11", "SKETCH", 0, 0, 0, True, 0, Nothing, 0)
boolstatus = Part.Extension.SelectByID2("3DSketch12", "SKETCH", 0, 0, 0, True, 0, Nothing, 0)
boolstatus = Part.Extension.SelectByID2("3DSketch13", "SKETCH", 0, 0, 0, True, 0, Nothing, 0)
boolstatus = Part.Extension.SelectByID2("3DSketch14", "SKETCH", 0, 0, 0, True, 0, Nothing, 0)
boolstatus = Part.Extension.SelectByID2("3DSketch15", "SKETCH", 0, 0, 0, True, 0, Nothing, 0)
boolstatus = Part.Extension.SelectByID2("3DSketch28", "SKETCH", 0, 0, 0, True, 0, Nothing, 0)
Part.ClearSelection2 True

boolstatus = Part.Extension.SelectByID2("3DSketch2", "SKETCH", 0, 0, 0, False, 8193, Nothing, 0)
boolstatus = Part.Extension.SelectByID2("3DSketch6", "SKETCH", 0, 0, 0, True, 16385, Nothing, 0)
boolstatus = Part.Extension.SelectByID2("3DSketch7", "SKETCH", 0, 0, 0, True, 24577, Nothing, 0)
boolstatus = Part.Extension.SelectByID2("3DSketch8", "SKETCH", 0, 0, 0, True, 32769, Nothing, 0)
boolstatus = Part.Extension.SelectByID2("3DSketch9", "SKETCH", 0, 0, 0, True, 40961, Nothing, 0)

boolstatus = Part.Extension.SelectByID2("3DSketch26", "SKETCH", 0, 0, 0, True, 8194, Nothing, 0)
boolstatus = Part.Extension.SelectByID2("3DSketch11", "SKETCH", 0, 0, 0, True, 16386, Nothing, 0)
boolstatus = Part.Extension.SelectByID2("3DSketch12", "SKETCH", 0, 0, 0, True, 24578, Nothing, 0)
boolstatus = Part.Extension.SelectByID2("3DSketch13", "SKETCH", 0, 0, 0, True, 32770, Nothing, 0)
boolstatus = Part.Extension.SelectByID2("3DSketch14", "SKETCH", 0, 0, 0, True, 40962, Nothing, 0)
boolstatus = Part.Extension.SelectByID2("3DSketch15", "SKETCH", 0, 0, 0, True, 49154, Nothing, 0)
boolstatus = Part.Extension.SelectByID2("3DSketch28", "SKETCH", 0, 0, 0, True, 57346, Nothing, 0)

Dim myFeature As Object
Set myFeature = Part.FeatureManager.SetNetBlendCurveData(0, 0, 0, 0, 1, True)
Set myFeature = Part.FeatureManager.SetNetBlendCurveData(0, 1, 0, 0, 1, True)
Set myFeature = Part.FeatureManager.SetNetBlendCurveData(0, 2, 0, 0, 1, True)
Set myFeature = Part.FeatureManager.SetNetBlendCurveData(0, 3, 0, 0, 1, True)
Set myFeature = Part.FeatureManager.SetNetBlendCurveData(0, 4, 0, 0, 1, True)
Set myFeature = Part.FeatureManager.SetNetBlendDirectionData(0, 32, 0, False, False)
Set myFeature = Part.FeatureManager.SetNetBlendCurveData(1, 0, 0, 0, 1, True)
Set myFeature = Part.FeatureManager.SetNetBlendCurveData(1, 1, 0, 0, 1, True)
Set myFeature = Part.FeatureManager.SetNetBlendCurveData(1, 2, 0, 0, 1, True)
Set myFeature = Part.FeatureManager.SetNetBlendCurveData(1, 3, 0, 0, 1, True)
Set myFeature = Part.FeatureManager.SetNetBlendCurveData(1, 4, 0, 0, 1, True)
Set myFeature = Part.FeatureManager.SetNetBlendCurveData(1, 5, 0, 0, 1, True)
Set myFeature = Part.FeatureManager.SetNetBlendCurveData(1, 6, 0, 0, 1, True)
Set myFeature = Part.FeatureManager.SetNetBlendDirectionData(1, 32, 0, False, False)
Set myFeature = Part.FeatureManager.InsertNetBlend2(2, 5, 7, False, 0.0001, False, True, True, True, False, -1, -1, False, -1, False, False, -1, False, -1, True, False)
Set CWAddinCallBackObj = Nothing
Set COSMOSWORKSObj = Nothing
End Sub
```